Layered vanadium and molybdenum oxides: batteries and electrochromics†

Natasha A. Chernova,[a] Megan Roppolo,[a] Anne C. Dillon[b] and M. Stanley Whittingham*[a]

Received 5th November 2008, Accepted 29th January 2009
First published as an Advance Article on the web 4th March 2009
DOI: 10.1039/b819629j

The layered oxides of vanadium and molybdenum have been studied for close to 40 years as possible cathode materials for lithium batteries or electrochromic systems. The highly distorted metal octahedra naturally lead to the formation of a wide range of layer structures, which can intercalate lithium levels exceeding 300 Ah/kg. They have found continuing success in medical devices, such as pacemakers, but many challenges remain in their application in long-lived rechargeable devices. Their high-energy storage capability remains an encouragement to researchers to resolve the stability concerns of vanadium dissolution and the tendency of lithium and vanadium to mix changing the crystal structure on cycling the lithium in and out. Nanomorphologies have enabled higher reactivities to be obtained for both vanadium and molybdenum oxides, and with the latter show promise for electrochromic displays.

1. Introduction

There has been much interest in the oxides of vanadium, molybdenum and tungsten because of the ready reversible incorporation of protons or alkali ions into their lattices to form electronically conducting bronzes.[1] These insertion reactions take place with a large free energy of formation, which has led to their use as the cathodes of lithium batteries. Concomitant with the ion insertion, electrons are introduced into the conduction bands giving rise to their dramatic colors, which can be related to the concentration of conduction electrons.[2] This ready coloration under ambient conditions led to their proposed[3] and actual use, particularly of tungsten trioxide, in electrochromic displays, where the intercalating ion is electrochemically inserted into or removed from the lattice. This feature article will be concerned with the oxides, and briefly some phosphates, of vanadium and molybdenum that have layered structures. We will discuss the relationship between their structures and properties, in particular their electrochemical behavior as relevant to batteries and electrochromics. The impact of morphology and size—bulk vs. nano—will be described, as there is presently much interest in nano-sized particles for diffusion controlled reactions where diffusion length and properties, such as the phase diagram, may be a function of size; however, nano is not always the right direction to go.[4]

The layered structures of vanadium and molybdenum contain predominantly MO_6 octahedra, with tetrahedra being less common. These octahedra normally share corners and/or edges (and in a few cases faces), to form two-dimensional sheet structures. These sheets may be one octahedron thick as in V_2O_5 itself

[a]*Chemistry and Materials, State University of New York at Binghamton, Binghamton, NY, 13902, USA. E-mail: stanwhit@gmail.com*
[b]*National Renewable Energy Laboratory, 1617 Cole Boulevard, Golden, CO, 80401-3393, USA*

† This paper is part of a *Journal of Materials Chemistry* theme issue on Layered Materials. Guest editors: Leonardo Marchese and Heloise O. Pastore.

Natasha A. Chernova

Natasha A. Chernova received her BS (1996) and MS (1998) in Materials Science, and her PhD (2001) in Physics from M. V. Lomonosov Moscow State University, Russia. She received a one-year fellowship from Corning Inc. in 2001 to work with Professor Eric Cotts at Binghamton University on microcalorimetry and thermodynamics of metals and alloys. She joined Professor M. Stanley Whittingham's group in 2002 where she studies transition metal oxides and phosphates as electrode materials for lithium ion batteries, with focus on structure and magnetic properties as a complementary tool for structural characterization.

Megan Roppolo

Megan Roppolo received her BS in Chemistry and French from St. Lawrence University in 2005 and is currently completing her PhD in Materials Chemistry in Professor Whittingham's group at Binghamton University. Her research area is the synthesis and characterization of amine-templated layered vanadium oxides, including vanadium oxide nanotubes, nanourchins, and $(enH_2)V_7O_{16}$. She is President of the local student chapter of the Materials Research Society.

or two octahedra thick as in the δ-phases, $M_xV_4O_{10}$. Both the MoO_6 and the VO_6 octahedra tend to be distorted with the bond lengths varying from 1.67 to 2.33 Å in MoO_3; the VO_6 octahedra tend to be even more distorted appearing more like a square pyramid with one very long V–O bond (2.1–2.6 Å, and 2.79Å in V_2O_5 itself) and a short vanadyl bond, –V=O (1.55–1.75 Å).[5] It is this structural characteristic of vanadium that leads to the large number of layered structures that it forms, as in the layered form of VO_2, where the VO_5 square pyramids share their four basal edges with other pyramids with the vanadyl groups alternating up and down.[6] V_2O_5 has the same structure, but with whole rows of –V=O groups absent in an ordered manner. The structures of some of the simpler oxides of vanadium and molybdenum are shown in Fig. 1 in polyhedral form. In the following sections, we will discuss in more detail several structures. Two recent review articles describe the vanadium oxide open framework structures,[5] and the synthesis of a number of layered vanadium oxides.[7] The oxides of molybdenum have been less studied, and for background the reader is referred to recent reviews.[8]

As noted above, when these oxides are intercalated by electron-donating cations, they become good conductors, and even metals. This gives them the special characteristic of being mixed conductors, showing both ionic and electronic conductivity. They are therefore ideal as the electrodes for electrochemical cells, potentially being fully reversible to both ions and electrons. One of their first uses was in the measurement of the ionic conductivity of the fast ion conductor, sodium β-alumina $NaAl_{11}O_{17}$; in this case, the layered $Na_xV_2O_5$ and Na_xWO_3 were used as the reversible electrode and allowed the measurement of the conductivity from liquid nitrogen temperatures to 800 °C.[9] In the 1970s there was much interest in developing rechargeable lithium batteries. V_2O_5[10–12] and α-MoO_3[13] were two of the first materials studied, and initially it was thought that they reacted by the removal of oxygen to give a lower oxide and Li_2O, rather than by an intercalation reaction.[10] Intercalation reactions are the mechanism in all consumer rechargeable batteries in commercial practice in 2009. Thus, in the search for electrode materials, most effort has centered on materials with structures that can intercalate small cations without major structural changes occurring. There are several recent reviews of battery materials.[14–16] Lithium-ion batteries are the current power sources of choice for portable electronics, offering high energy density and longer lifespan than comparable technologies. Furthermore, Li-ion technologies have sufficient specific energy and power densities to meet the desired targets for hybrid electric vehicles (HEVs) and plug-in hybrid electric vehicles (PHEVs) for up to a 40 mile range. However, significant improvements in lifetime, especially at high rate, for inexpensive, safe and non-toxic electrode materials are still needed before Li-ion batteries are employed for large-scale application in the transportation sector. Increasing the energy density of electrode materials will also enable an extended battery range for PHEVs and eventually allow fully electric vehicles. Batteries are also essential for the full use of intermittent power sources, such as solar and wind.

Materials to be used for electrochromic applications must fulfill many of the same criteria as battery electrodes, they must be able to react very fast with small cations such as hydrogen or lithium and totally reversibly. However, as they are used as thin films, weight is not an issue so heavier elements such as molybdenum and tungsten can be used. Ideally they should also be very good electronic conductors, as one cannot mix in an opaque conductor such as carbon as used in batteries, because the optical behavior would be badly degraded.

In the published literature, a number of different units are commonly used in describing the discharge or charge current in electrochemical cells. The most common are mA/cm^2, mA/g and C rate. In the first the rate describes the actual current used divided by the geometric area of the electrode material, not the surface area. The second is the current used divided by the weight of material, and can be unrealistically high if a very low material loading is used; typical loadings of commercial lithium cells approach 20 mg/cm^2. The C rate is a derived quantity, and describes how long it takes to fully discharge the cell; C rate is 1 hour, C/10 is 10 hours. In this feature article, we will generally

Anne C. Dillon

Anne C. Dillon is currently a Principal Scientist at the National Renewable Energy Laboratory (NREL). She received BS degrees in both chemistry and history from the Massachusetts Institute of Technology in 1988 and a PhD in physical chemistry from Stanford University in 1993. Her research at NREL is focused on the synthesis and characterization of novel nanostructured materials including: single- and multi-wall carbon nanotubes as well as metal oxide nanorods and particles. The nanostructures are targeted for a variety of renewable energy applications with an emphasis on hydrogen sorption materials, electrical energy storage and electrochromic windows.

M. Stanley Whittingham

M. Stanley Whittingham received undergraduate and graduate degrees from Oxford University, UK. He spent 4 years in Materials Science at Stanford University studying ion transport in solids, then joined Exxon Research to study the mechanism of the redox reduction of solids by lithium which led to the use of intercalation compounds as battery electrodes in the mid-1970s. In 1988 he became Professor of Chemistry at Binghamton, building a program emphasizing the use of soft chemistry approaches to synthesize advanced and nano materials. He has received the Young Author Award, the Battery Research Award and was elected a Fellow of the Electrochemical Society.

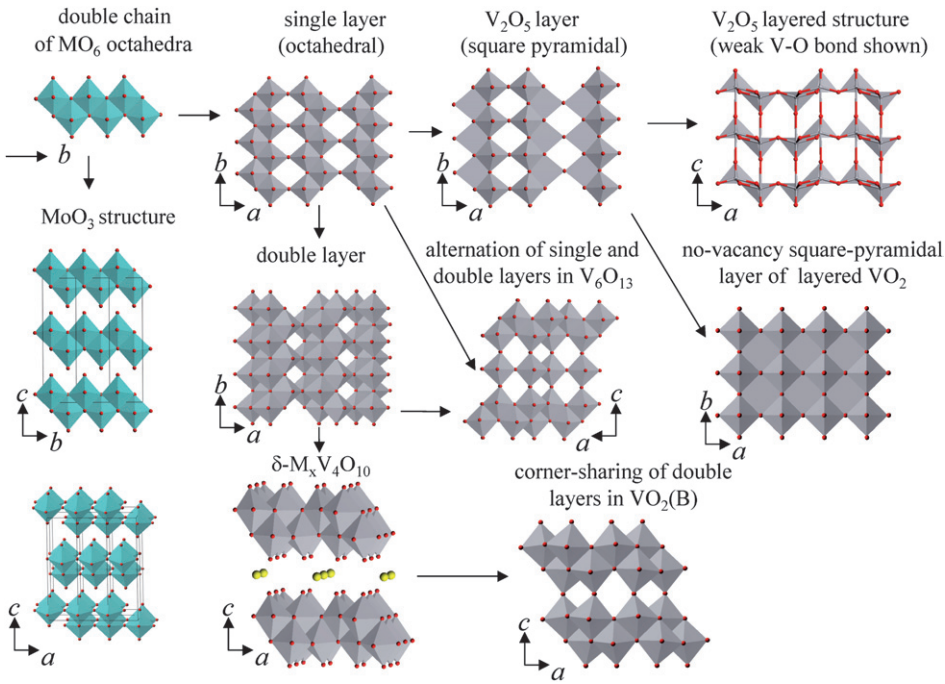

Fig. 1 Structural relations between molybdenum and vanadium oxides.

use the units of the original paper, but where possible also use mA/cm^2. In describing the structures in this feature article, we will use the *c* parameter to describe the lattice parameter perpendicular to the layers in the structure.

2. Vanadium oxides

Comparison of MO_3, single- and double-layer V_2O_5 and V_6O_{13} structures

Most of the vanadium and molybdenum oxides possess layered or open structures and show rich crystal chemistry due to a variety of oxidation states, coordination polyhedra and metal–oxygen connectivity.[5] V_2O_5 and MoO_3 both have a layered type of structure and d^0 electronic configuration of the transition metals. The basic building unit of these oxides is a double chain of edge-sharing MO_6 (M = Mo, V) octahedra as presented in Fig. 1. In the MoO_3 structure[17] (orthorhombic, space group *Pcmn*, $a = 3.963$ Å, $b = 3.696$ Å, $c = 13.855$ Å), these chains extending along the *b*-axis are connected back-to-back to form the double layers in the *ab*-plane (Fig. 1). The MO_6 octahedron in MoO_3 is significantly distorted. Only the corner-sharing octahedra along the double chains are connected by equal 1.94 Å Mo–O bonds; in the *c*-direction, the terminal bond is the shortest (1.67 Å) while the opposite bond is the longest (2.33 Å); in the *a*-direction another short bond (1.73 Å) alternates with a long (2.25 Å) bond. Thus, there is a clear tendency towards molybdenyl MO_2^{2+} formation. MoO_3 can host various species in the interlayer space forming molybdenum bronzes.[8] It intercalates about 1.5 Li/Mo with structure retention, but the reaction kinetics in bulk material are too slow for practical applications.

When the double chains are connected through the side corners, a single layer occurring in many vanadium oxide structures is formed (Fig. 1). In α-V_2O_5 (orthorhombic, space group *Pmmn*, $a = 11.512$ Å, $b = 3.564$ Å, $c = 4.368$ Å),[18] one of the terminal bonds is a short vanadyl bond, while the other V–O distance is much longer: 2.79 Å. It is usually considered as a weak bond, so that the vanadium coordination polyhedron becomes a square pyramid. The apices of the VO_5 pyramids alternate in an up-up-down-down sequence in the V_2O_5 with every third row being vacant due to the corner sharing of the double chains; in layered VO_2, which will be discussed later, every row is occupied. The weak V–O interaction provides the layered character of the structure (Fig. 1).

A double layer typical of δ-type vanadium oxides is formed from single sheets with all the apices (vanadyl bonds) up in one layer and down in the other layer. These single sheets are connected back to back by edge sharing along the weak V–O bond, which is shorter than in V_2O_5, thus leaving all vanadyl bonds terminal (Fig. 1). To avoid confusion with δ-LiV_2O_5 and to underline the double layer nature of this structural type we will refer to it as δ-$M_xV_4O_{10}$.[5] This layer is present in a variety of vanadium oxide gels and δ-type layered compounds offering high electrochemical capacity. These structures intercalate lithium in a single- or a two-phase manner depending on the nature of interlayer species, stacking distance, crystallinity and morphology. Single and double layers alternate in the V_6O_{13} structure sharing corners (Fig. 1),[19] which provides several sites for lithium intercalation. When two double layers of the δ-$M_xV_4O_{10}$ structure collapse upon the removal of the interlayer species, a metastable form of vanadium dioxide VO_2(B) is formed (Fig. 1).[20] In the following sections we will consider lithium intercalation in these and related structures with the emphasis on structural changes, bulk vs. nanosized comparison, and practical applicability.

Lithium insertion in crystalline V_2O_5

Initially, about 1% of lithium is intercalated in crystalline V_2O_5 forming α-$Li_xV_2O_5$; the ε-phase with increased puckering of V_2O_5 layers is formed for $0.35 < x < 0.7$. At the LiV_2O_5 composition, gliding of every other layer in the *b*-direction leads to the δ-phase. These transformations do not affect the strong V–O bonds and are fully reversible. Intercalation of 0.5 Li per V corresponds to a specific capacity of 147 mAh/g, comparable to that of $LiCoO_2$, which also can cycle about 0.5 Li without irreversible phase changes. However, the performance at high current densities and cycling stability of $LiCoO_2$ is far better than that of V_2O_5.[16] The irreversible transformation to the γ-phase occurs when more than 1 lithium is intercalated. In the γ-phase, the layers are severely puckered and the square pyramid apices alternate in the up-down-up-down sequence. These structural transitions are reflected in the discharge curve of V_2O_5 as three plateaus at 3.4, 3.2, and 2.3 V for the α/ε, ε/δ, and δ/γ two-phase regions, respectively (Fig. 2). The γ-$Li_xV_2O_5$ phase can itself be reversibly cycled for $0 \leq x \leq 2$ corresponding to a theoretical capacity close to 300 mAh/g. Upon further reduction, below 1.9 V, the ω-$Li_3V_2O_5$ phase with a tetragonal structure is formed ($a = 4.1$ Å, $c = 9.2$ Å).[21] According to Delmas, after one electrochemical cycle, the tetragonal superstructure disappears, and a disordered rock-salt structure with a lattice parameter of 4.1 Å is formed. Tetragonal ω-$Li_3V_2O_5$ may also be obtained by chemical lithiation of V_2O_5 in n-butyllithium; the subsequent delithiation by bromine in acetonitrile gives a cubic phase with a very high cationic vacancy content.[21] Leger *et al.* reported that the tetragonal superstructure of ω-$Li_xV_2O_5$ is preserved upon cycling which is reversible in the limits $0.4 \leq x \leq 2.65$, providing a capacity of 310 mAh/g at a C/20 rate.[22] The increase of current density results in a noticeable decrease of the amount of lithium cycled (Fig. 2) due to kinetic limitations for deep discharge. Impedance spectroscopy reveals a decrease of the lithium diffusion coefficient D_{Li} from around 3.3×10^{-9} cm^2 s^{-1} for low lithium content ($0.4 \leq x \leq 0.7$) to 10^{-10} cm^2 s^{-1} for $x = 2$ to a value as low as 10^{-12} cm^2 s^{-1} for the maximum lithium content of 3. Moreover, vanadium dissolution was observed at higher discharge rates, also limiting the electrochemical capacity and reversibility of the material. However, excellent cyclability was obtained when moderate discharge rates were used with capacities of 250 mAh/g after 40 cycles. This is perhaps due to the advantageous morphology of V_2O_5 produced by the heat-treatment of $V_2O_5 \cdot nH_2O$ gel, which is usually formed as nano-fibers as will be discussed later.

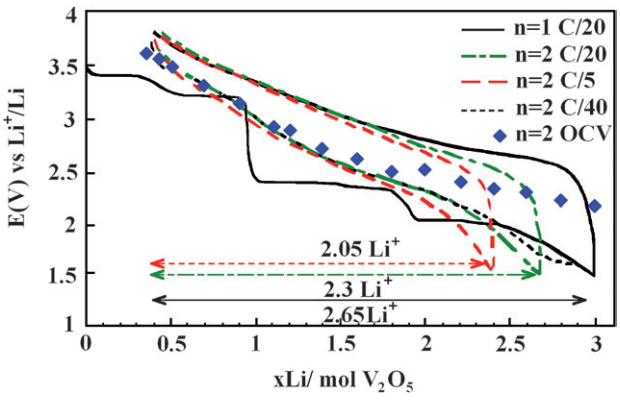

Fig. 2 Electrochemical cycling of V_2O_5 and ω-$Li_3V_2O_5$ at various current densities. Modified with permission from C. Leger, S. Bach, P. Soudan, and J.-P. Pereira-Ramos, *J. Electrochem. Soc.*, 2005, **152**, A236–A241. Copyright The Electrochemical Society 2005.

Vanadium pentoxide gels

Vanadium oxides produced in gel forms show greatly improved reactivity. Synthesis methods and properties of vanadium oxide gels have been reviewed by Livage,[23,24] Wang and Cao,[25] and Rolison and Dunn.[26] For electrochemical applications, the most employed synthesis approaches are acidification of a vanadate solution using ion-exchange resin with subsequent spontaneous polymerization of the resulting HVO_3 solution[27,28] and hydrolysis and condensation of vanadium alkoxides.[29,30] The composition of the resulting gel is $H_xV_4O_{10} \cdot nH_2O$ suggesting a partial reduction of the vanadium. The V^{4+}/V^{5+} ratio can vary from as low as 1% up to 20% while still preserving the structure.[23] Morphologically, the gels consist of entangled vanadium oxide ribbons about 0.5 mm long, 10 nm wide and 10 Å thick forming pores filled with liquid electrolyte (Fig. 3). Depending on the drying process three main types of solids are produced. If water is removed by simple evaporation, surface tension causes the porous network to collapse and xerogels with surface areas of 1–10 m^2/g are formed.[23] Exchanging the water with acetone or other solvent and subsequent drying by liquid CO_2 under supercritical (no surface tension) conditions preserves the porous morphology and gives the most electrochemically active aerogels with surface areas of 350–400 m^2/g.[28] Aerogel-like materials often termed ambigels are obtained by a multi-step sequence of solvent exchange and evaporation of the last solvent (with minimal

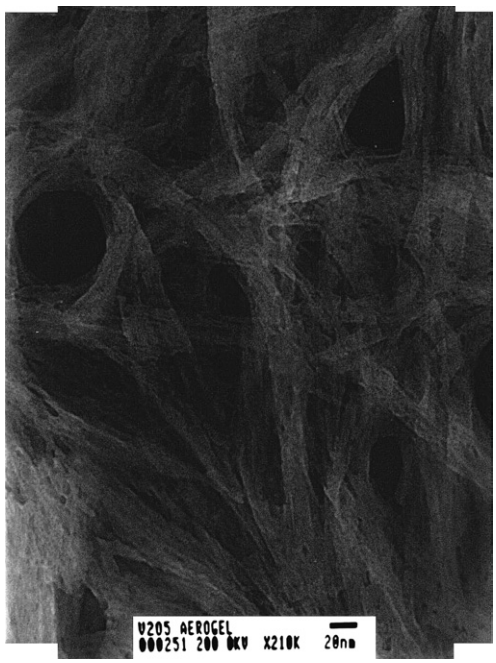

Fig. 3 TEM image of V_2O_5 ambigel, bar is 20 nm. Reproduced with permission from J. S. Sakamoto and B. Dunn, *J. Electrochem. Soc.*, 2002, **149** A26–A30. Copyright The Electrochemical Society 2002.

surface tension) under ambient conditions.[31] Ambigels preserve a high surface area of 100 to 300 m^2/g with reactivity and properties close to those of aerogels.

Ambiently dried xerogels usually contain n = 1.8 water in the formula $H_xV_4O_{10}\cdot nH_2O$ leading to an interlayer distance of 11.5 Å.[32] Vacuum-drying at 100 °C as routinely used by Smyrl's group gives xerogels with n = 0.5 and a stacking distance of 8.8 Å.[33] Aerogels and ambigels usually show larger interlayer distances varying from 10.5 to 14 Å depending on the type of the residual organic solvent.[34] The amount of strongly bound water in aerogels is small (n = 0.2–0.3) as compared to xerogels.[27,28] The structure of dried gels has been a subject of debate between the single-layer α-V_2O_5 proposed by Livage[23] and the double-layer δ-$M_xV_4O_{10}$ types proposed by Smyrl.[35] The pair-distribution function analysis of the X-ray scattering data done for a xerogel provided solid evidence for the double-layer δ-type structure.[36] No such studies were performed for aerogels, and they are assumed to have a similar double-layer structure. The reactivity of xerogels and, especially, aerogels varies significantly not only with the synthesis method, but also with the electrode preparation determining such critical parameters as interlayer spacing, ribbon crystallinity and orientation, and the active surface area. For the fundamental studies, Smyrl used thin (1–10 μm) dip-coated or spin-coated electrodes on conductive substrates. Ambiently dried dip-coated electrodes have vanadium oxide ribbons oriented in the *ab* plane, so that X-ray diffraction reveals only a set of 00*l* peaks; spin-coated electrodes show increased orientation disorder, less crystallinity, and higher electrochemical capacities.[33,37] The Dunn group introduced sticky carbon electrodes providing high surface area, intimate electrical contact for each particle and improved accessibility for the electrolyte.[31,38]

Using spin-coated electrodes or chemical lithiation with n-BuLi it was found that xerogels can react with 4 Li per mole of V_2O_5. For the aerogels, the same capacity was originally reported (Fig. 4),[28] but later they were found to react with up to 5.8 Li.[39] The corresponding low-rate capacities of 560 and 650 mAh/g for xerogels and aerogels, respectively, exceed by far the 170 mAh/g for $LiFePO_4$,[40] and about 275 mAh/g theoretically possible in layered $LiMO_2$ materials.[16] The equilibrium voltage–composition curves presented in Fig. 4 suggest different mechanisms of lithiation for xerogels and aerogels. For the xerogel, the voltage decreases continuously with the amount of inserted Li to about 1.8 V for x = 4, which is typical for a single-phase intercalation reaction. X-Ray absorption studies of xerogels indicate a progressive reduction of the vanadium upon lithiation.[41] In contrast, for the aerogel, a voltage plateau at about 2.8 V is observed up to the highest Li content.[39] XPS and XAS data show nearly no effect of the Li content on the vanadium oxidation state in aerogels.[39,42] XANES data indicate that the most pronounced change in vanadium coordination in aerogels is the lengthening of the vanadyl bond. This suggests that Li might be coordinated to the former vanadyl oxygen, probably, as in the case of Cu^{2+} and Zn^{2+}-containing gels, which will be discussed later.[43,44] However, it remains unclear how the charge transfer occurs. Such unusual lithiation behavior seems to be the result of extremely high surface area, large interlayer spacing and the nearly amorphous structure of aerogels, which is preserved in Smyrl's studies by employing spin-coated electrodes without any heat treatment. Rolison and Dunn observed that surface defects such as vanadium vacancies might be important for this lithiation mechanism.[26]

The active material loadings and current densities in the experiments described above are much too low for practical applications. Thus, the standard composite electrodes with active xerogel or aerogel material pressed together with some form of conductive carbon and polymer binder were studied.[45–47] The performances of the xerogel and aerogel-based composite electrodes fell short compared to the thin-film electrodes, especially at high current densities (Fig. 5).[33] For example, xerogel-based electrodes intercalate only 2 Li per V_2O_5.[45] Freeze-dried aerogel-like solids intercalate up to 2.7 Li per V_2O_5 at a 1C rate corresponding to intercalation of 1 Li per V_2O_5 per hour in an electrode of 1.3 cm^2 area with about 10 mg of active material, and up to 4 Li under the GITT regime.[46] Some vanadium dissolution

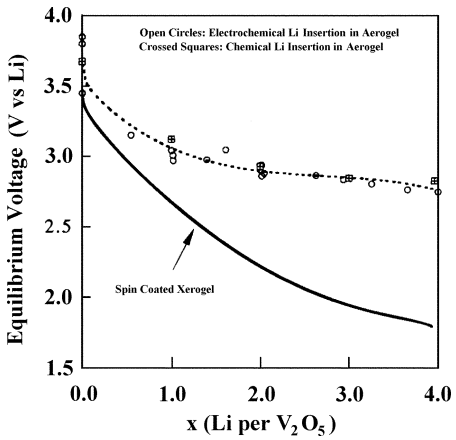

Fig. 4 Equilibrium voltage–composition curves for V_2O_5 xerogel and aerogel, determined by the electrochemical GITT method, or by chemical lithiation. 1 M $LiClO_4$/propylene carbonate, 25 °C. Reproduced with permission from D. B. Le, S. Passerini, J. Guo, J. Ressler, B. B. Owens and W. H. Smyrl, *J. Electrochem. Soc.*, 1996, **143**, 2099–2104. Copyright the Electrochemical Society 1996.

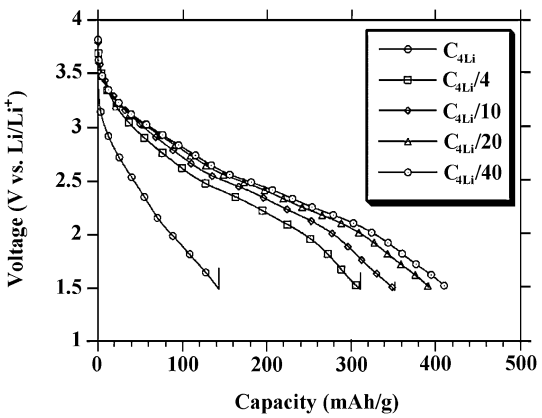

Fig. 5 Voltage vs. capacity curves of a composite electrode with aerogel-like active material at different current rates. C rate corresponds to 560 mAh/g (4 Li per V_2O_5) per hour. Actual current densities in these experiments vary from 0.13 to 5.20 mA/cm^2. Reproduced with permission from B. B. Owens, S. Passerini and W. H. Smyrl, *Electrochim. Acta*, 1999, **45**, 215–224. Copyright Elsevier Science 1999.

was found if the discharge voltage was below 2 V, causing capacity fading upon cycling, which is consistent with an earlier report.[48] Stable cycling with a reversible capacity of 125 mAh/g was achieved at 1C rate in the voltage window 2.5 to 4 V.[46] The composite electrodes with vanadium aerogel as the active material show a continuous voltage decrease with lithium insertion (Fig. 5).[33,49] Depending on the degree of crystallinity, the electrochemical curve may be nearly featureless as for a single-phase reaction[47] or show two-phase plateaus usually at 2.5 and 2.1 V.[46] XAS studies by Mansour *et al.* revealed vanadium reduction upon electrochemical lithium insertion in composite electrodes.[47,50] Mansour *et al.* also investigated the problem of capacity fading with cycling for $V_2O_5 \cdot 0.5H_2O$ aerogels and ambigels by X-ray absorption spectroscopy. The depth of vanadium reduction upon discharge was found to decrease with cycle number. Changes in the vanadium coordination suggested the irreversible formation of electrochemically inactive phases.[51,52]

The reasons for the deterioration of the electrochemical activity of the composite electrodes are quite straightforward: reduced surface due to the particle agglomeration and collapse of the porous morphology, increased crystallinity, and altering of the surface by carbon, which is likely to occur during the electrode preparation involving pressing and heat-treatment. Thus, to employ the unique characteristics of the nanostructured vanadium oxide gels novel approaches to the electrode architecture are required. The Dunn group has made some progress in this area by replacing carbon black with single-wall carbon nanotubes which are close in size and morphology to the vanadium oxide ribbons. The resulting nanocomposite reveals lower electrical resistivity resulting in higher rate capability and more stable cycling (Fig. 6).[53] Hierarchical electrodes based on inverted opal structures were developed by the same group in the hope of improving mass transport and reducing polarization.[54] The choice of electrolyte is another critical issue for optimizing the electrochemical performance of nanomaterials.[4] A conventional $LiPF_6$ electrolyte component may decompose releasing hydrofluoric acid causing cathode dissolution. Formation of nanosized

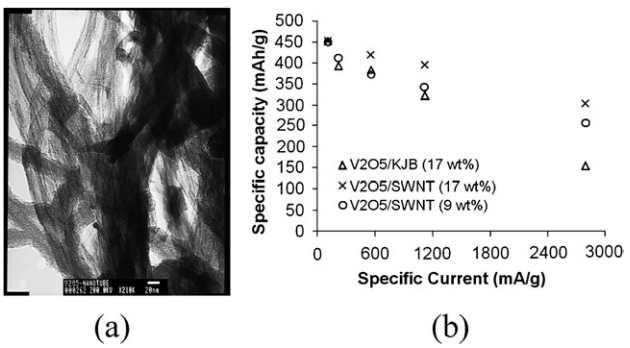

Fig. 6 (a) TEM image of V_2O_5 aerogel-single wall carbon nanotube (SWNT) composite; the scale bar is 20 nm. (b) Specific capacity as a function of specific current for intercalation electrodes containing V_2O_5 aerogels: circles = V_2O_5/SWNT (9 wt.%), crosses = V_2O_5/SWNT (17 wt.%); triangles = V_2O_5/Ketjen black (17 wt.%) electrodes. The cathode loading is 1–2 mg V_2O_5/cm^2. Reproduced with permission from J. S. Sakamoto and B. Dunn, *J. Electrochem. Soc.*, 2002, **149** A26–A30. Copyright The Electrochemical Society 2002.

deposits was found upon cycling V_2O_5 thin films in a $LiPF_6$/PC electrolyte, while no such deposit occurred in a $LiClO_4$-based electrolyte.[55]

Vanadium oxide gels readily intercalate other species, such as Na^+, Ag^+, Mg^{2+}, Ca^{2+}, Cu^{2+}, Zn^{2+}, Ba^{2+} and Al^{3+}.[23,56–58] Mn ions were introduced into gels by adding a Mn source to the ion-exchange resin,[59] as well as by chemical[60] and electrochemical[61] oxidation of $VOSO_4$. Interestingly, the equilibrium voltage–composition curves for polyvalent cation (Mg^{2+}, Zn^{2+}, and Al^{3+}) insertion do not strongly depart from that of Li, suggesting that the vanadium oxide host dictates the energetic of the process.[57] In electrochemical tests, the polyvalent ions were transported between the working and counter electrodes suggesting that high-energy intercalation batteries based on Mg^{2+}, Al^{3+} and Zn^{2+} may be feasible.[26,57] Amatucci has also demonstrated the reversible electrochemical insertion of polyvalent cations (Ca^{2+}, Mg^{2+}, Y^{3+}) into V_2O_5 nano-powders produced by the combustion flame-chemical vapor condensation process.[62] He suggested that the measured capacity for the reactions with polyvalent cations are in part due to pseudocapacitive surface reactions concurrent with guest ion intercalation into the bulk structure.

XAS studies of Cu and Zn contained aerogel-like materials revealed that both guest metals occupy square planar sites being coordinated by four apical oxygens of the same V_2O_5 layer. Such coordination leaves the interlayer spacing clear, and Cu-doped aerogel-like materials show excellent cycling stability of 170 mAh/g for over 450 cycles (specific current: 136 mA/g, current density: 0.15 mA/cm^2).[33] The reversible conversion of Cu^{2+} to metallic copper remarkably increases the electronic conductivity of this material, which is important for cycling stability.[63] However, the same question as in the case of lithiation of high-surface area aerogels remains: where does the charge go upon the increase of metal M content in $M_xV_4O_{10}$? For $M^{2+}{}_{0.25}V_2O_5$ (M = Cu, Zn; $x \leq 0.25$) compositions studied, 1/8 of V^{4+} should occur, while XAS data do not show any significant variation of the oxidation state with M content.[43,44,56,64] A plausible explanation for this may be the presence of protons on the structure, in such amounts that the total charge of protons and metal ions remains constant.

Surprisingly, NMR studies which could provide local structural information and are very sensitive to the change of magnetic field at the vanadium ions (V^{5+} is non-magnetic, while V^{4+} has spin S = 1/2) are scarce for vanadium oxide gels.[65–67] Studies of the lithiation process of Smyrl's aerogels by the combination of ^{7}Li, ^{51}V NMR and ESR suggests that at least up to 2 Li intercalated per V_2O_5, lithium ions are located at apical oxygens as was discussed earlier. Progressive vanadium reduction to 4+ is observed in this composition range in EPR spectra. Upon further lithiation, lithium is forced to occupy different sites and this process is not yet fully understood. Further vanadium reduction still occurs, but the amount of V^{3+} ions becomes less than expected. It is speculated that the charge transfer to the non-bridging oxygen ions may occur as ^{7}Li NMR suggests that lithium ions, not neutral atoms, are intercalated.[65] Thus, the lithiation of aerogels appears to be partially an insertion, and partially a pseudocapacitive process. In papers by Holland *et al.*[66,67] a peak at nearly 0 ppm is found in the ^{7}Li MAS NMR spectra of xerogels with protons being ion-exchanged with lithium, which is consistent with the presence of a small fraction

of V^{4+} ions. Upon further lithiation, a peak at higher ppm is developing and getting broader with increasing lithium content. This peak can be attributed to Li ions with a progressively increasing number of V^{4+} ions in the coordination sphere. Quantitative analysis of such spectra would be interesting.

Crystalline δ-phase vanadium oxides

The same materials with improved crystallinity can be formed by hydrothermal reactions; the structures of these have been extensively studied by Galy,[68] Oka[69] and our Binghamton group.[70–72] These more crystalline forms with inorganic or organic cations between the V_4O_{10} sheets have shown greater reversibility than the gels with capacities[73–77] exceeding 200 mAh/g in some cases. In our recent review of these compounds[40] the positive effect of Mn and/or ammonium on the electrochemical behavior was highlighted.[75] The first cycle of $NH_4V_4O_{10}$ shown in Fig. 7(a) reveals multistep behavior reminiscent of V_6O_{13} to be discussed later in the paper and indicates that there are several different sites for the lithium. The capacity to 2.5 V is equivalent to total reduction of the vanadium to V^{4+} giving $Li_3NH_4V_4O_{10}$. This behavior is not necessarily observed in all crystalline double-sheet structures. $Fe_{0.2}TMA_{0.33}V_4O_{10}\cdot 0.33H_2O$ and $Zn_{0.84}V_4O_{10}$ materials show a smoother potential–composition behavior but with increased polarization and lower capacity.[73] However, the corresponding manganese compounds show much higher electrochemical capacities as shown in Fig. 7(b). Metal

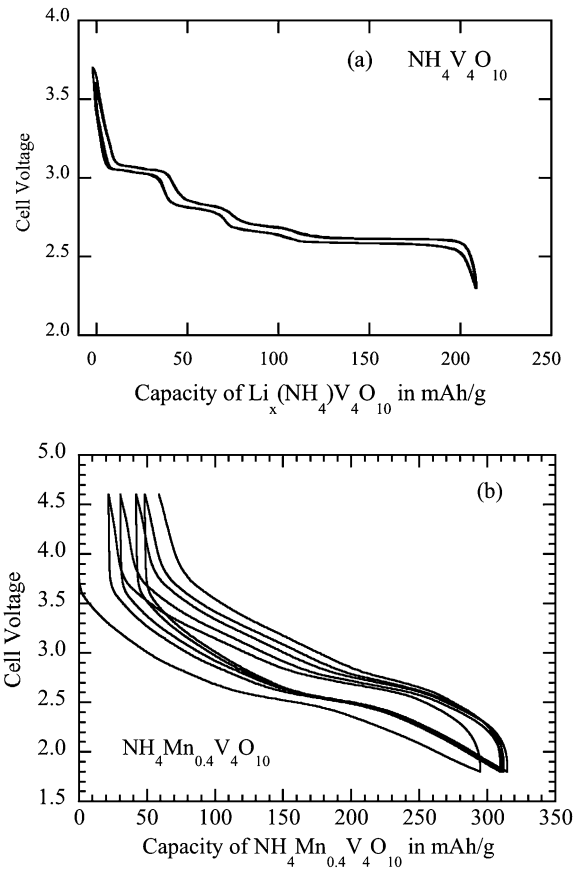

Fig. 7 Comparison of the cycling behavior of (a) $NH_4V_4O_{10}$ and $(NH_4)_yMn_zV_4O_{10}$.

and organic ions in these compounds occupy interlayer sites, as opposed to surface sites occupied by Cu^{2+} and Zn^{2+} in aerogels. It suggests that the surface area and, possibly, surface defects play an important role in site preferences of the intercalated metals. Further structural studies of the δ-phase materials are necessary to elucidate the structural changes upon lithium cycling, the role of Mn and ammonium ions in the improvement of the electrochemical performance, and the reasons for capacity fading.

Vanadium oxide gels–polymer materials

Conducting organic polymers such as polyaniline,[78,79] poly(pyrrole)[80] and poly(thiophene)[81] have been employed to enhance the electronic conductivity of the vanadium oxide layers of xerogels and aerogels. The synthetic approaches to these hybrid materials include simultaneous or consecutive polymerization of components. The simultaneous polymerization provides better morphology control and more homogeneous distribution.[26,82] In the case of xerogels, polymer was actually intercalated between the vanadium oxide slabs,[78] while in the case of aerogels an interpenetrating network of electrochemically active oxide and electronically conducting polymer was formed.[80] Strong interactions between the organic and inorganic components were evidenced in the FTIR spectra of the aerogel–polymer composite. As in the case of the pristine aerogels and xerogels, the electrochemical performance of the corresponding hybrids depends strongly on the preparation method. Surprisingly, not much improvement in electronic conductivity and electrochemical behavior has been achieved so far. The most promising, polyaniline–xerogel and post-oxidized polypyrrole–aerogel hybrids exhibit capacities of about 3 and 3.7 Li per V_2O_5, respectively, when tested at very low current densities in composite electrodes.[79,81]

In the Binghamton group, electrospun polymer or composite polymer–vanadium oxide fibers were used as templating agents for the hydrothermal synthesis of vanadium oxides with advantageous morphologies.[83–88] In the first approach, electrospun polyactide (PLA) or polymethacrylate (PMMA) fibers were added to the NH_4VO_3 solution with pH adjusted to 3.3–4 by acetic acid. A room-temperature sol-gel process resulted in coated polymer fibers, while hydrothermal treatment at 160 °C gave double-layer $(NH_4)_xV_2O_{5-\delta}\cdot nH_2O$ fibers [Fig. 8(a)]. The PMMA-assisted fibers were found to be more electrochemically active with an initial discharge capacity of 250 mAh/g [Fig. 8(b)]. On the subsequent charge not only was all the Li removed but the ammonium ions as well. A smooth charge–discharge curve is observed for this compound, in contrast to crystalline $NH_4V_4O_{10}$. In the second approach, adopted after ref. 89, a solution of vanadium triisopropoxide (VOIP) and PMMA was electrospun to produce composite fibers. The fiber diameter varied from 250 nm to a micron as the VOIP concentration increased. The exact nature of this composite is under investigation, XRD data reveal a nearly amorphous layered structure with 10.7 Å spacing. Upon hydrothermal treatment at pH 2–3 adjusted by acetic acid this fibrous precursor converts into $H_xV_4O_{10}\cdot nH_2O$ ($x \leq 0.48$; $n \leq 2.0$) nanorods with double-layer structure similar to that of vanadium oxide gels. However, the lithium insertion capacity of this material is significantly less than

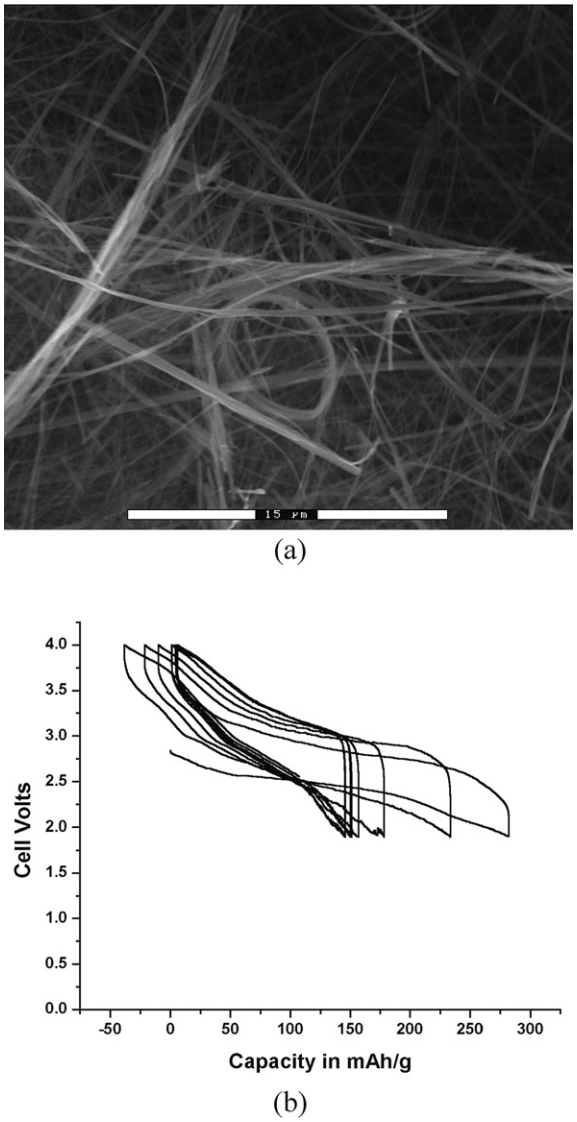

Fig. 8 (a) SEM image (scale bar is 15 μm) and (b) cycling behavior of $(NH_4)_xV_2O_{5-\delta}\cdot nH_2O$ fibers synthesized in the presence of PMMA. Reproduced with permission from S. T. Lutta, H. Dong, P. Y. Zavalij and M. S. Whittingham, *Mater. Res. Soc. Symp. Proc.*, 2004, **788**, L5.5.1–L5.5.6. Copyright the Materials Research Society 2004.

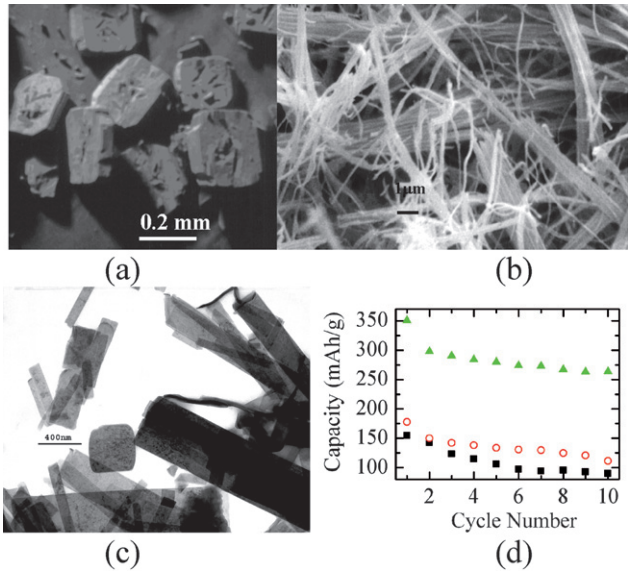

Fig. 9 SEM images of (a) Aldrich V_2O_5, (b) V_2O_5 fibers synthesized using electrospun PLA fibers as a template, scale bar is 1μm, (c) V_2O_5 rods synthesized from composite PMMA–vanadium oxide electrospun fibers, scale bar is 400 nm. (d) Cycling performance of (a), (b), and (c) plotted as squares, circles, and triangles, respectively. Voltage windows are 2 to 3.5 V for (a) and (b), and 1.75 to 4 V for (c). Current density is 0.1 mA/cm^2 with cathode loading about 25 mg/cm^2 for (a) and (b), and 5 mg/cm^2 for (c). Plot (a) is reproduced with permission from S. T. Lutta, H. Dong, P. Y. Zavalij and M. S. Whittingham, *Mater. Res. Bull.*, 2005, **40**, 383–393. Copyright Elsevier 2004.

that of gels. If the pH is adjusted to the same value by oxalic acid, VO_2(B) nanorods are formed (see Fig. 1 for the structure).

Nano-forms of crystalline V_2O_5

Xerogels, aerogels and composite electrospun fibers with double-layer structure can be converted to nano-crystalline V_2O_5 by simply annealing in oxygen. Generally, nanostructured V_2O_5 shows better electrochemical performance than the bulk counterpart due to facile strain relaxation upon Li cycling, shorter Li diffusion lengths, and higher surface area. The evolution of the cycling ability of V_2O_5 with morphology changing from micro- to nano-crystalline is presented in Fig. 9, which is based on the results obtained in the Binghamton group. The best capacity and cycling stability is demonstrated by the V_2O_5 nanorods synthesized by the annealing of the above-mentioned $H_xV_4O_{10}\cdot nH_2O$ ($x \leq 0.48$; $n \leq 2.0$) nanorods in oxygen.[86–88] Similar results were obtained by Dunn and Tarascon for the vanadium oxide aerogel annealed in oxygen.[46] By increasing the annealing temperature from 200 to 300 °C and annealing time from 25 to 38 minutes, the evolution of the cycling curves from a smooth single-phase curve typical of aerogel, to a multi-step curve at the first discharge typical of crystalline V_2O_5 was observed. The reversible capacity of ω-$Li_3V_2O_5$ eventually produced by the deep discharge of these compounds was about 300 mAh/g. The rate capability of V_2O_5 synthesized directly by heating $H_xV_2O_5\cdot nH_2O$ gel was discussed earlier in the paper (Fig. 2).[22] Nano-crystalline V_2O_5 can also be synthesized from sol-gel precursors using porous templates with subsequent annealing.[90–94] The synthesis and intercalation properties of such nano-V_2O_5 and related materials were recently reviewed.[25] Polycrystalline V_2O_5 nanorods 115 nm in diameter and 2 μm in length synthesized using polycarbonate membrane were subjected to extensive rate-capability tests.[91] In the voltage range of 2.5 to 3.6 V corresponding to the reversible α → ε → δ transformations (see Fig. 2) almost one Li per formula unit is cycled at C/20 rate (0.47 μA cm^{-2}). The charge and discharge curves show the same phase transitions as in the bulk samples. At 10C rate (0.09 mA cm^{-2}) 0.9Li and at 1000C rate (9 mA cm^{-2}) about 0.4 Li can be intercalated. The rate capability of the nanostructured electrode is much higher than that of the thin (250 nm) V_2O_5 film studied in the same work, which intercalates less than 0.2 Li at 1000C rate (Fig. 10). The volumetric capacity

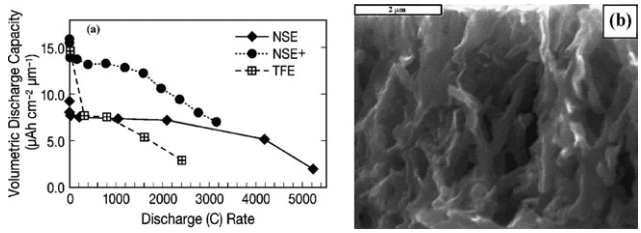

Fig. 10 (A) Comparison of volumetric capacity versus discharge rate for different V_2O_5 electrodes. NSE is the nanostructured electrode prepared from the etched 50 nm pore diameter template; NSE+ is the nanostructured electrode to which additional sol-gel precursor was added after template synthesis; and TFE is the thin-film control electrode. The lowest discharge rates and corresponding current densities are 2.4 μA/cm^2 (C/20), 3.4 μA/cm^2 (C/24) and 4.67 μA/cm^2 (C/22) for NSE, NSE+, and TFE, respectively. The capacities for the slowest discharge are around 147 mAh/g for all the materials. (B) SEM image of the NSE+ (side view). Reproduced with permission from C. J. Patrissi and C. R. Martin, *J. Electrochem. Soc.*, 2001, **148**, A1247-A1253. Copyright the Electrochemical Society 2001; and from C. R. Sides, N. Li, C. J. Patrissi, B. Scrosati and C. R. Martin, *Mater. Res. Soc. Bull.*, 2002, **27**, 604–607. Copyright the Materials Research Society 2002.

of these materials is limited by cathode loading dictated by the membrane geometry. Some improvement has been achieved by etching the polycarbonate membrane, which increases the number of pours and, therefore, nanorods per unit of area (Fig. 10).[92,93] Single-crystalline V_2O_5 nanorods with improved rate capability were obtained by electrochemical deposition inside a polycarbonate membrane.[94]

Structure and electrochemistry of V_6O_{13}

An alternation of single and double vanadium oxide layers occurs in V_6O_{13} (Fig. 1), a compound with mixed $V^{+4.33}$ oxidation state. The valence-bond sum calculations suggest single layer sites [V(1)] are occupied by V^{4+} as well as V(3) sites of the double layer presented in Fig. 11(b) in gray, while V(2) sites [highlighted octahedra in Fig. 11(b)] of the double layer possess more V^{5+} character. The maximum lithium uptake by V_6O_{13} corresponds to the reduction of all vanadium to the trivalent state giving the high theoretical energy density of about 900 Wh/kg; moreover, the compound is metallic at room temperature.[95] Due to the

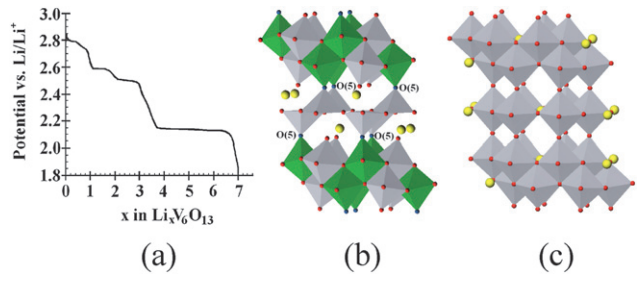

Fig. 11 (a) Discharge curve of a Li | liquid electrolyte | V_6O_{13} "coffee-bag" type cell. Crystal structure of (b) $Li_2V_6O_{13}$, the V(2) sites containing V^{4+} ions in V_6O_{13} and oxidized upon initial stages of Li intercalation are highlighted; (c) $Li_3V_6O_{13}$. Panel (a) is reproduced with permission from H. Björk, S. Lidin, T. Gustafsson and J. O. Thomas, *Acta Cryst.*, 2001, **B57**, 759–765. Copyright International Unit of Crystallography 2001.

combination of high electrochemical capacity and electronic conductivity, V_6O_{13} has been considered as an excellent candidate for the cathode material since the original work of Murphy in 1979.[96]

V_6O_{13} has a low-temperature polymorph, the structure of which has been a subject of controversy.[97–100] The phase transition at 150 K is accompanied by a drop of electrical conductivity and magnetic susceptibility, suggesting that charge redistribution occurs along with the structural changes. According to the recent single crystal data by Höwing *et al.*,[101] the most significant structural changes occur in the single vanadium sheet, where V(1a) atoms located on one side of the double chains experience a displacement of 0.21 Å along the *b*-axis (see octahedral single layer in Fig. 1), while V(1b) atoms in the other half of the double chain shift by only 0.06 Å, which leads to the loss of the symmetry center. Our bond valence sum calculations suggest that the V(1a) atoms become more V^{5+}-like in the low-temperature phase, and the V(2a) atoms of the double layer, which share a corner with the V(1a) tend to slightly decrease their charge.

Murphy *et al.* conducted detailed investigation of the electrochemical properties of several vanadium oxide phases including $V_6O_{13\pm y}$.[102] One of the most important results of this work was the recognition that the non-stoichiometry has a critical effect on the reaction of vanadium oxides with lithium. For example, stoichiometric V_6O_{13} can incorporate up to 4.5 Li per formula unit when immersed into n-butyllithium solution, while slightly oxidized V_6O_{13+y} reacts more intensively incorporating up to 8 Li. The electrochemical capacity of V_6O_{13+y} is also larger than that of its stoichiometric analog, suggesting that the limiting factor is the electron count, not the availability of lithium insertion sites. In later works it has been shown that V_6O_{13} can electrochemically incorporate up to 8 Li per formula unit, with all the V being reduced to the 3+ oxidation state.[103,104] The intercalation of lithium proceeds through several phase changes as illustrated by the electrochemical curve in Fig. 11(a) and is accompanied by a decrease of the electrical conductivity. It was also found that deep discharge leads to an increased irreversibility due to loss of electrode integrity and side reactions.

The lithiated $Li_xV_6O_{13}$ phases were examined by various techniques, including cyclic voltammetry and impedance spectroscopy,[103] powder X-ray diffraction,[104] magnetic measurements and X-ray absorption studies.[105] The detailed single-crystal diffraction studies revealed $Li_xV_6O_{13}$ phases with $x = 0.67$, 1, 2, and 3.[106–108] In these phases, the vanadium–oxygen framework of V_6O_{13} is maintained with lithium initially intercalated between the single and double layers at chemically equivalent sites with five-fold oxygen coordination [Fig. 11(b)]. In $Li_{0.67}V_6O_{13}$, the intercalation occurs at every third double chain, resulting in triple the unit cell size of V_6O_{13}; in LiV_6O_{13}, the Li ions appear in every other double chain, resulting in a doubling of the original unit cell. Finally, in $Li_2V_6O_{13}$, all the fivefold sites are occupied by Li ions; the unit cell becomes similar to that of V_6O_{13} but expanded by 7.6% in the direction perpendicular to the layers (*c*-axis). An analysis of the V–O bonding reveals that the initial reduction occurs at former V(2) sites of the double layer, which are highlighted in Fig. 11(b).[109] It is accompanied by the elongation of the V–O bond extending towards the single sheet V(2)–O(5) and by the decrease of the V^{4+}–V^{4+} distance. As the length of the V(2)–O(5) bond increases,

the length of the V(1)–O(5) bond decreases and this bond becomes double. Correspondingly, the opposite V–O distance increases to the extent that the corresponding bond becomes weak. Therefore, the coordination of the V(1) atoms located next to the intercalated Li becomes square pyramidal. Thus, the initial intercalation of lithium occurs in the single vanadium sheets, while the extra electrons are transferred to the double layer of VO_6 octahedra. In $Li_2V_6O_{13}$, where all the vanadium is 4+, the single layer becomes similar to that of V_2O_5 with an up-up-down-down sequence of square pyramidal chains. The formation of $Li_3V_6O_{13}$ is accompanied by a significant rearrangement of the Li ions [Fig. 11(c)]. In the single vanadium oxide layer, the Li ions are now located in the square-planar sites with 50% occupancy, while in the double layer, Li ions fully occupy square-pyramidal sites. The unit cell in $Li_3V_6O_{13}$ contracts in the *c*-direction as compared to the $Li_2V_6O_{13}$ almost to the size of the parent V_6O_{13} compound and expands by 5.6% in the *b*-direction in comparison with V_6O_{13}.

The four phase transitions, decrease of electronic conductivity upon lithium insertion, and the loss of electrode integrity made it difficult to attain good cyclability for V_6O_{13} cells. The solution was found in using polymer electrolytes providing the internal bonding to the cathode and anode. A loss of discharge capacity from over 7 to about 4 Li per formula unit was found over the first 10 cycles, but almost no capacity fading was observed in the following 100 cycles using $LiCF_3SO_3$/PEO electrolyte at 155 °C.[103] Valence Technology showed that the reversible capacity faded from 7 to about 5 Li per V_6O_{13} after 180 cycles with a polymer electrolyte at room temperature (charge at 0.25 mA/cm^2, discharge at 1 mA/cm^2 between 3.0 and 1.8 V vs. Li/Li$^+$).[110] HydroQuebec developed a polymer battery technology based on vanadium oxide and formed Avistor in a joint venture with Kerr McGee to commercialize it. The Avistor cell contained a lithium metal anode and VO_x cathode with a polyethylene oxide (PEO)-imide salt (LiTFSI) electrolyte.[111] The system operated from 60 to 90 °C providing a good energy storage capability of 333 Wh/l and 205 Wh/kg. Cells demonstrated stability for over 500 cycles and good power capability.[112] However, a restricted battery cycling life and fire-creating lithium shorting has led to the demise of this technology. In a recent report by Leger *et al.*, $Cr_{0.36}V_6O_{13.50}$ synthesized by heating of Cr-exchanged vanadium oxide gel under reducing atmosphere demonstrated an initial capacity of 370 mAh/g, sustaining about 320 mAh/g after 35 cycles at low current rates.[113] However, the role of Cr doping and the morphology of the material are not clear from the paper.

Layered VO_2

Closely related to the V_2O_5 layered structure is a polymorph of VO_2 synthesized by the dehydration and electrochemical delithiation of $Li_{0.6}V_{2-\delta}O_{4-\delta}\cdot H_2O$.[6,114] In this compound, layers with idealized composition V_2O_4 have no vacancies and the pyramids are arranged in the up-down-up-down chess-board-like manner [Fig. 1 and Fig. 12(a)]. Neutron diffraction studies indicated that lithium is located between the water molecules and VO_5 pyramid bases, as well as at some of the vanadium sites. The comparison of calculated and measured densities suggests that 10–15% of the vanadium sites are vacant. Thus, this vanadium

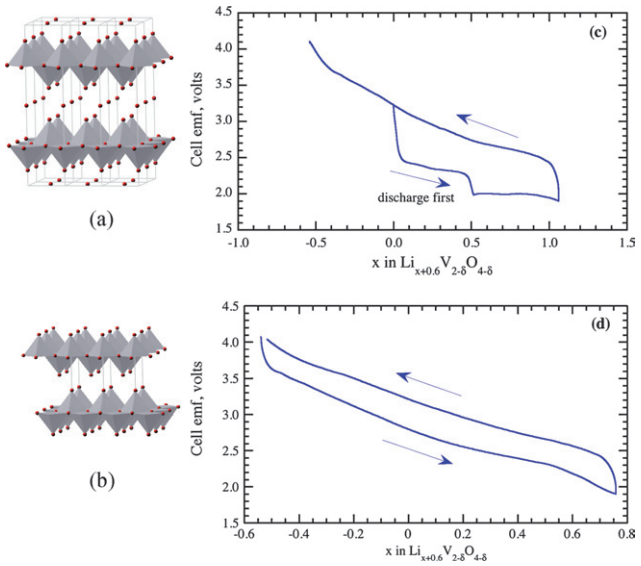

Fig. 12 Structure and electrochemical properties of $Li_{0.6}V_{2-\delta}O_{4-\delta}\cdot H_2O$: (a) stacking of layers in the hydrated form; (b) layer glide and the reduction of interlayer distance in the anhydrous $V_{2-\delta}O_{4-\delta}$. Electrochemical discharge and recharge of the $Li_{0.6}V_{2-\delta}O_{4-\delta}$ at 0.2 mA/cm^2, (c) first cycle and (d) second. Panels (c) and (d) are reproduced with permission from T. Chirayil, P. Zavalij and M. S. Whittingham, *J. Electrochem. Soc.*, 1996, **143**, L193–L195. Copyright the Electrochemical Society 1996.

oxide exhibits vanadium deficiency and Li/V disorder. Upon dehydration, the layers glide with respect to each other, so that the vanadyl oxygen of one layer occupies the former site of water oxygen above the pyramid base of the next layer [Fig. 12(b)].

The electrochemical reduction of the $Li_{0.6}V_{2-\delta}O_{4-\delta}$ compound is shown in Fig. 12(c). About 0.5 lithium is incorporated in the first step and another 0.5 lithium is incorporated above a cutoff of 2 V. On the following recharge, all the intercalated lithium as well as the 0.6 lithium originally in the structure is removed. Subsequently, more than 1.3 lithium is reversibly cycled in a single-phase manner, suggesting that the crystal structure has been changed [Fig. 12(d)]. If the cell is subjected to a charge step first, all the Li is removed quantitatively, with a sharp end point, to give $V_{2-\delta}O_{4-\delta}$, which in its ideal form has the composition of vanadium dioxide, VO_2. This phase can reversibly intercalate about 1Li/V above a cutoff of 2 V.

Nano-structured forms of VO_2

The electrochemical characteristics of the rutile form of VO_2 have been studied,[115–117] and little if any lithium could be incorporated into the bulk structure. However, a nanostructured monoclinic rutile form is electrochemically active with stable cycling at 120 mAh/g.[118] Another form of VO_2, the metastable VO_2(B), has a structure closely related to that of the layered vanadium oxide gels. In VO_2(B) the double layers of V_4O_{10} type are not separated with intercalated species, but share corners to form a shear-type structure containing one-dimensional tunnels.[5,20,119] This structure starts to transform irreversibly to the thermodynamically stable rutile phase above 350 °C.[120] VO_2(B) readily intercalates lithium by reaction with

n-butyllithium (up to 0.75 Li/V) and electrochemically (up to 0.5 Li/V with a two-phase plateau at 2.5 V for $0.14 < x < 0.5$).[102,121] Dahn investigated VO_2(B) as a cathode for aqueous Li-ion batteries,[122–124] and revealed that saturation of the electrolyte of appropriate pH (between 8 and 10) with dissolved vanadium species results in good capacity retention. Nanostructured VO_2(B) with particle size about 100 nm was synthesized by reduction of aqueous potassium or lithium vanadate solution with potassium borohydride and/or sodium dithionite at pH 4.[120,125] VO_2(B) nanorods with 40–60[126] and 80–250[127] nm diameters were obtained by a surfactant-assisted hydrothermal method. These materials show an initial capacity at or above 300 mAh/g (equivalent to 1 Li/V) retaining about 250 mAh/g after 15–20 cycles when cycled between 3.5–4 and 1–1.5 V with a current density about 0.5 mA/cm^2. The room-temperature reduction products show nearly featureless discharge curves with just a hint of plateau at 2.5 V, while the nanorods show a pronounced plateau at 2.5 V, which suggests better crystallinity. Tarascon investigated nanotextured VO_2(B) produced by heating vanadium oxide aerogels in vacuum.[128] Varying the annealing temperature between 280 and 400 °C, materials with surface areas from 185 to 122 m^2/g were obtained. Particle size estimated from the X-ray diffraction pattern using the Scherrer formula increases from 6 to 20–25 nm with the annealing temperature. The 280 °C product, which has the smallest particle size, shows capacities in excess of 500 mAh/g between 4 and 1.5 V, which fade rapidly with cycling due to vanadium dissolution at low voltages.[46,128] Stable performance at 175 mAh/g was obtained by cycling between 4 and 2.4 V. It is interesting to note that the 280 °C product cycling curve is very reminiscent of the aerogel cycling, but with an even less pronounced 2.5 V plateau. With increased particle size, the 2.5 V plateau develops as well as another plateau at 2.1 V, which is similar to the cycling behavior of bulk VO_2(B).[121] The ease of transformation of aerogels to VO_2(B) suggests similar double vanadium oxide layers in both structures.

Vanadium oxide nanotubes

The vanadium oxide nanoscroll, also referred to as a vanadium oxide nanotube (VONT), was first reported by Spahr *et al.*[129] as a novel vanadium oxide morphology with potential applications in the construction of lithium-ion batteries.[130] Compared with other vanadium oxides, the nano size and anisotropic tubular morphology of the VONTs give them the added benefits of a large surface area (with reactive sites outside the tube, inside the tube, and at the tube openings as pictured in Fig. 13), a short diffusion path in the solid, and an electrolyte-filled channel to quickly transport the lithium ions to the insertion sites. The VONTs are created by an amine-templated reaction that takes place under hydrothermal conditions.

Krumeich *et al.*[131] described the synthesis conditions and method used to produce VONTs from vanadium(V) triisopropoxide. A wide range of amine templates was used, including aliphatic primary amines with alkyl chain lengths between 4 and 22 CH_2 groups long and aliphatic α,ω-diamine templates, ($H_2N(CH_2)_nNH_2$), with $n = 14$ to 20. Vanadium oxide fibers and lamellar structured composites were formed when using amines outside these length parameters. At the first stage of the synthesis, vanadium(V) triisopropoxide and the chosen amine are combined in absolute ethanol and then hydrolyzed, which results in an orange composite after 12 to 96 hours of aging. The composite is then treated hydrothermally at 180 °C for 2 to 7 days, resulting in a black VONT product.

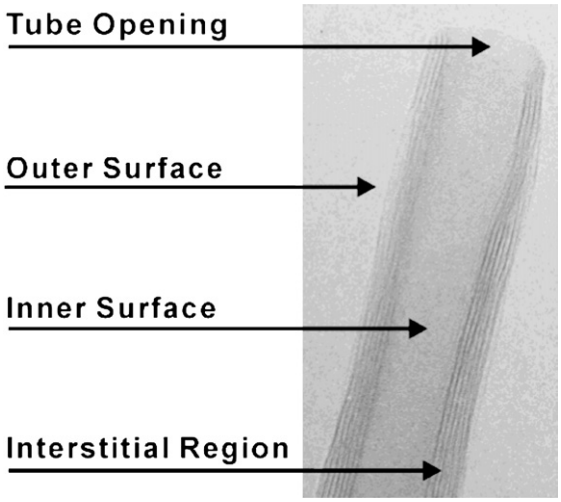

Fig. 13 TEM of VONT showing four topological sites. Reproduced with permission from H.-J. Muhr, F. Krumeich, U. P. Schönholzer, F. Bieri, M. Niederberger, L. J. Gauckler and R. Nesper, *Adv. Mater.*, 2000, **12**, 231–234. Copyright WILEY-VCH 2000.

This synthesis was improved upon by the discovery that V_2O_5 and $VOCl_3$ are also possible vanadium starting materials for the formation of VONTs.[132] These starting materials result in VONTs with the same structure and morphology as those synthesized using vanadium alkoxides, but with the advantages of being cheaper to produce, less sensitive to the ambient atmosphere, and easier to scale up into a large reaction. The structure of the precursor formed after the aging of a mixture of V_2O_5 and dodecylamine before hydrothermal treatment was studied.[133] Within the first few minutes of the aging reaction it is obvious that this precursor consists of a new layered product with a different XRD pattern than that of the initial starting materials. The presence of distinct 00l peaks at low values of 2θ indicate that layers, with an interlayer spacing of 26.4 Å, are formed during this step. The interlayer distance does not change significantly during the subsequent hydrothermal treatment. FTIR data suggest that the amine in the precursor may be completely or partially protonated, but the color and the magnetic susceptibility studies suggest that V is present in the V^{5+} oxidation state.

The synthesis produces VONTs, both isolated and grown together, as the exclusive product with diameters of 15–100 nm, inner tube diameters of 5–50 nm, and lengths up to 15 μm. The open-ended nanotubes consist of alternating layers of vanadium oxide intercalated with the amine surfactant. During the hydrothermal treatment, the layers will form either a series of concentric tubes or a scrolled morphology (Fig. 14). Cross-sectional TEM images in Fig. 15 show that the "ideal" concentric tubes are rarely seen (<1%) unless the tube is composed of fewer than five layers.[131] The dimensions of the VONTs were found to be controlled by the structure-directing template, as monoamine

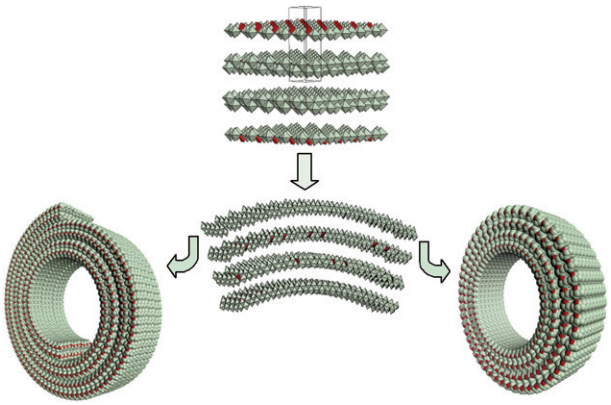

Fig. 14 Schematic representation of vanadium oxide scroll formation. Reproduced with permission from V. Petkov, P. Y. Zavalij, S. Lutta, M. S. Whittingham, V. Parvanov and S. Shastri, *Phys. Rev. B*, 2004, **69**, 085410. Copyright The American Physical Society 2004.

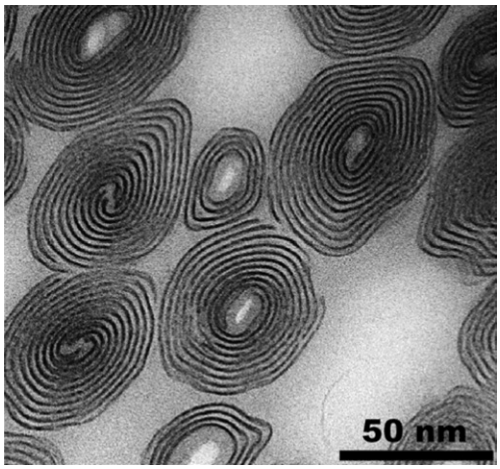

Fig. 15 TEM of cross sections of VONTs with hexylamine template. Reproduced with permission from H.-J. Muhr, F. Krumeich, U. P. Schönholzer, F. Bieri, M. Niederberger, L. J. Gauckler and R. Nesper, *Adv. Mater.*, 2000, **12**, 231–234. Copyright WILEY-VCH 2000.

templates tend to form wide tube openings with tube walls consisting of 2 to 10 vanadium oxide layers while diamines generally lead to tubes with thicker walls and a larger number of layers (>10). The interlayer spacing depends upon the length of the intercalating amine (between 1.7 and 3.8 nm).

The VONTs are highly flexible and retain their morphology when the amine template is removed or exchanged with other ions. Attempts at amine removal through calcination were only successful under an inert atmosphere.[85] Nesper's group found that the template could be partially removed under mild acidic conditions.[129] They also reported template-free VONTs created by refluxing in a saturated solution of NaCl in ethanol for 24 hours.[134] These structures exhibited a reduced interlayer spacing of 8.6 Å, compared to 28–30 Å for regular VONTs and 11 Å for Na^+ ion exchanged VONTs,[135] but maintained the VONT morphology. The VONTs were also found to retain their tubular morphology when ion-exchanged with a variety of cations, including NH_4^+,[129] Na^+, K^+, Mg^{2+}, Ca^{2+}, Sr^{2+}, Fe^{2+}, Co^{2+}, Ni^{2+}, Cu^{2+},[135] and Mn^{2+},[133] though only manganese has been shown to completely exchange all of the amine. After the exchange, the interlayer distance decreases significantly in all cases, in the range of 9.7 to 12.7 Å, with the final value being dependent upon the size of the metal ion being intercalated. Though the overall tube morphology is preserved, often defects are introduced into the structure in many cases. These defects may cause damage to the tube walls, but also make the tube more resistant to the electron beam in TEM studies due to the increased proximity of the vanadium oxide layers.[135] It is also possible to exchange monoamines for diamines in a ratio of two monoamines replaced by every one diamine.[131]

The VONT walls probably possess a unique double layer structure[133] that was first reported for $BaV_7O_{16}\cdot nH_2O$[136] (Fig. 16). In this structure, two sheets of edge-sharing vanadium oxide distorted octahedra are connected by vanadium oxide tetrahedra located between the sheets. These layers are stacked in the [001] direction. The coordination of the atoms in the layer involves three different vanadium sites: V(1) and V(2) distorted octahedra and V(3) tetrahedra. The layer can also be described as two sheets of square pyramids linked together by weak V–O bonds.[5] Each sheet in the double layer is made up of zigzag chains formed by the trans edge sharing of a trimer of polyhedra. Each of these chains is connected into a layer by the corner sharing of one oxygen atom, leaving two of the five octahedral sites vacant. The tetrahedra are located in the windows formed by these four empty sites (two each from the bottom and top layers).

The V_7O_{16} layer has a unit cell parameter of $a = 6.16$ Å, which remains the same despite the size of the template or metal ion that is present between the layers, as expected for an intercalation compound. This indicates that the structure is stable, as is proved by the stationary hk0 peaks in the XRD pattern of

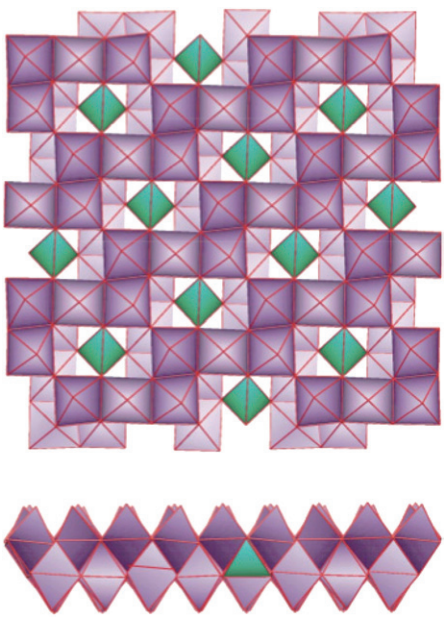

Fig. 16 Structure of the vanadium oxide layer in BaV_7O_{16}. Reproduced with permission from P. Y. Zavalij and M. S. Whittingham, *Acta Cryst.*, 1999, **B55**, 627–663. Copyright International Union of Crystallography 1999.

ion-exchanged samples. It was due to this steady unit cell parameter of $a = 6.16$ Å that the VONT structure was initially linked to that of BaV_7O_{16}. The determination of the structure of the VONT walls proved difficult by normal crystallographic techniques because their tubular curvature results in a lack of three-dimensional periodicity and long-range order in the structure. For this reason, an atomic pair distribution function (PDF) technique was employed to overcome the limits of Bragg diffraction data, and the results are shown in Fig. 14.[137] This technique is sensitive to fine structural features and atomic ordering and can compare these parameters to those of a structural model. The structure of the vanadium oxide in $BaV_7O_{16}{\cdot}nH_2O$ was found to correspond most closely to the experimental data from the VONTs. One characteristic of the VONT wall structure that is still not fully understood is the charge distribution of the mixed V^{4+} and V^{5+} ions.

A new ethylene diammonium-containing phase was synthesized as another way of successfully studying the crystal structure of the VONT walls.[138] The advantage of this material, called $(enH_2)V_7O_{16}$, is that the short amine template prevents the rolling or scrolling of the layered vanadium oxide. The successful synthesis of pure-phase $(enH_2)V_7O_{16}$[139] allowed for a more in-depth characterization that revealed lattice parameters of $a = 6.167(2)$ Å, $b = 6.170(2)$ Å, $c = 19.107(5)$ Å and angles $\alpha = 96.062(7)°$, $\beta = 92.66(1)°$, $\gamma = 90.011(6)°$ for the plate-like crystals of 1–2 μm in size, pictured in Fig. 17(a). Another related structure, the vanadium oxide nanourchin,[140] is also the result of the scrolling of amine-templated vanadium oxide; however the dilute synthesis conditions allow the VONTs to grow from a single nucleation site, resulting in the sea urchin-like morphology [Fig. 17(b)]. The formation of this type of structure suggests that VONTs begin growing from a small amount of lamellar material and, after scrolling, continue to grow radially along the tube axis. The VONTs that make up the nanourchins are of particularly high quality, with few visible defects [Fig. 17(c)]. Structural characterization and magnetic properties are similar to those of typical VONTs.[139]

Magnetic studies of VONTs show Curie–Weiss paramagnetism at low temperatures and a spin-gap contribution at temperatures above 100 K.[139,141] The latter was explained by the presence of antiferromagnetic $S = ½$ dimers, which would consist of two edge- or corner-sharing V^{4+} ions that do not interact with other V^{4+} ions in the structure. The paramagnetic V^{4+} ions make up approximately 16% of the V in the materials. Though their location is not known precisely, this percentage correlates to the number of tetrahedral sites in the MV_7O_{16} structure, despite the fact that V^{4+} generally prefers square-pyramidal or octahedral geometry. Alternatively, the presence of the third contribution due to V^{4+} ions existing as trimers was suggested.[142] Formation of the itinerant charge carriers and room-temperature ferromagnetism has been reported for VONTs that are doped with lithium or iodine.[141] The composition and structure of the doped products were not characterized in the original work. These phenomena were not observed in our studies of lithiated VONTs.[143] In contrast, the optical studies of VONTs exchanged with Na^+, Zn^{2+}, and Mn^{2+} suggest that the charges injected into metal-exchanged VONTs are pinned due to Madelung energy effects.[144]

Despite early reports claiming poor performance and rapidly decreasing capacities,[134] VONTs were eventually shown to be viable as a cathode material in lithium ion batteries by Nordlinder *et al.*[145] Both the as-synthesized product (with dodecylamine and hexadecylamine templates) and a Na^+ ion-exchanged product were tested and showed reversible capacity for 100 charge and discharge cycles between 1.8 and 3.5 V with a current loading between 25 and 100 mA/g. The electrochemistry results showed that the lithium salt in the electrolyte played a large role in the capacity obtained. The amine-templated materials had somewhat lower capacities than the ion-exchanged samples, though the capacity of these ion-exchange cells, which used the lithium bistrifluoromethylsulfonyl imide (LiTFSI) electrolyte, decreased by 30% from an initial value of 250 mAh/g over the course of 100 cycles (Fig. 18). $LiBF_4$- and $LiPF_6$-containing electrolytes caused cell capacity to increase over 30 cycles from approximately 25–75 mAh/g until respective maximum values of 170 and 155 mAh/g were reached. Similarly, Mn ion-exchanged VONTs can also be intercalatively reduced by lithium ions, but with a capacity of only 140 mAh/g.[133] In this case, the tube retains its morphology, but because of the large change in interlayer distance from 26.6 to 10.52 Å, significant cracking occurs.

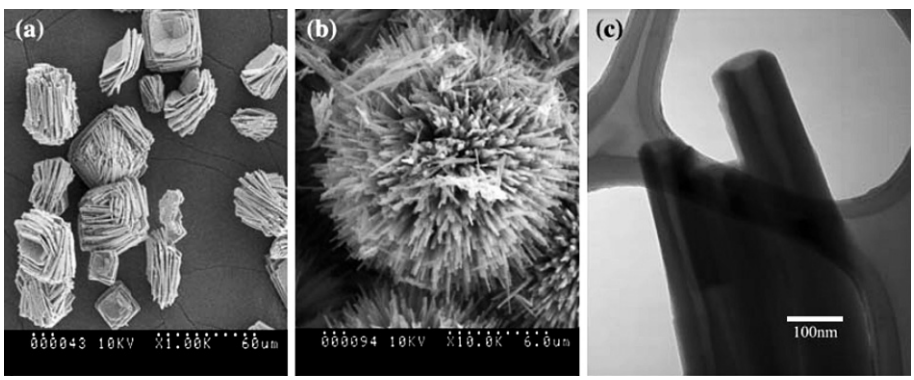

Fig. 17 (a) $(enH_2)V_7O_{16}$, (b) vanadium oxide nanourchins, and (c) close-up of VONTs within the nanourchin. Reproduced with permission from M. Roppolo, C. B. Jacobs, S. Upreti, N. A. Chernova and M. S. Whittingham, *J. Mater. Sci.*, 2008, **43**, 4742–4748. Copyright Springer Science + Business Media 2008.

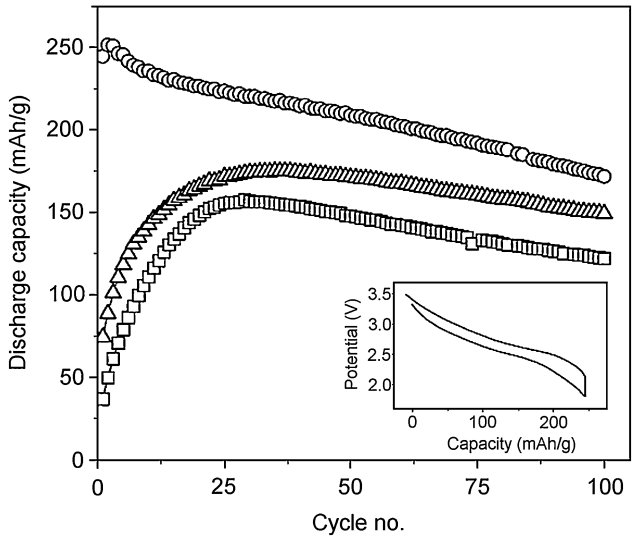

Fig. 18 Discharge capacities for cells cycled with three different salts in the electrolytes: LiTFSI (circles), $LiBF_4$ (triangles), and $LiPF_6$ (squares). The inset displays the first discharge/charge cycle for the cell cycled in LiTFSI electrolyte. The potential is given vs. Li/Li^+. Reproduced with permission from S. Nordlinder, K. Edström and T. Gustafsson, *Electrochem. Solid-State Lett.*, 2001, **4**, A129–A131. Copyright The Electrochemical Society 2001.

$Li_{1+x}V_3O_8$ and related structures

$Li_{1+x}V_3O_8$ has also been of interest as a cathode material in lithium batteries due to its ability to intercalate lithium ions between its layers. It is synthesized *via* several methods, including high-temperature melting,[146] sol-gel method,[147] and freeze-drying.[148] The LiV_3O_8 structure, which has been discussed in detail elsewhere,[5] is made up of quadruple chains of VO_6 octahedra connected through terminal corners by double chains of VO_5 square pyramids. Between these layers, lithium ions are found in fully occupied octahedral sites and in partially occupied tetrahedral sites as seen in Fig. 19(a). In 1983, Panero *et al.*[149] used $Li_{1+x}V_3O_8$ with low x values in a lithium cell and found that, at current densities ranging from 0.5 to 2 mA/cm^2, it would reversibly insert three lithium ions per formula unit with a steady capacity of more than 100 mAh/g over many cycles. According to the open-circuit voltage dependence upon Li content in $Li_{1+x}V_3O_8$, the lithiation proceed as a single-phase reaction for $1 + x \leq 3$, and a two-phase plateau appears up to $Li_4V_3O_8$ composition (Fig. 20),[150] which has a disordered rock-salt structure. Chemically, $Li_5V_3O_8$ composition can be achieved.[151]

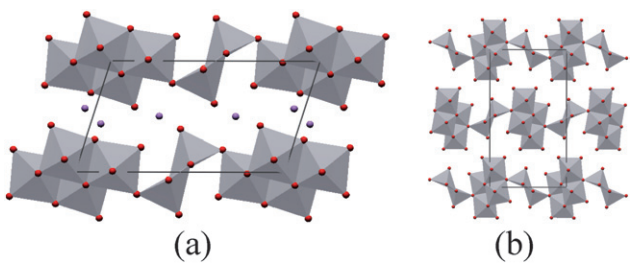

Fig. 19 Crystal structures of (a) $Li_{1+x}V_3O_8$ and (b) $H_2V_3O_8$.

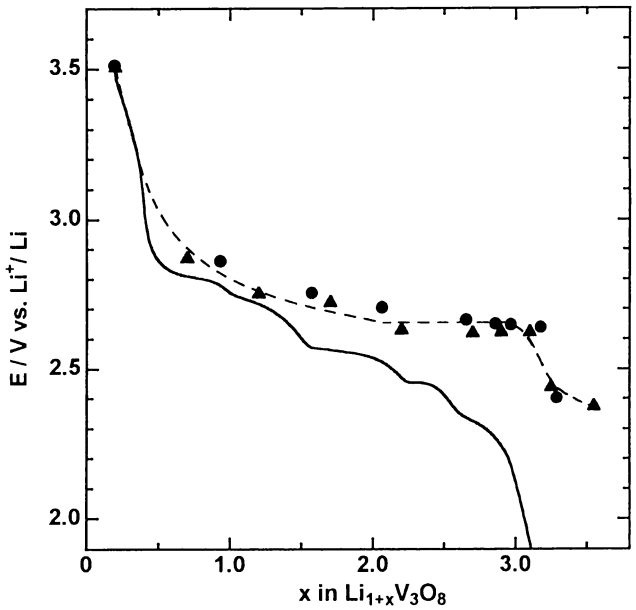

Fig. 20 Discharge curve at 0.1 mA/cm^2 at 25 °C, and OCP plots of $Li_{1.2}V_3O_8$: (circles) by chemical method at room temperature and (triangles) by electrochemical method at 25 °C. Reproduced with permission from J. Kawakita, Y. Katayama, T. Miura and T. Kishi, *Solid State Ionics*, 1998, **107**, 145–152. Copyright Elsevier Science 1998.

However, the discharge curves, as well as cycling voltammograms, show numerous features suggesting minor structural re-arrangements during Li insertion (Fig. 20 and 21). The phases formed as lithium is inserted into the $Li_{1+x}V_3O_8$ structure during battery cycling have recently been revisited using ^7Li and ^{51}V MAS NMR studies.[152] It was determined that the peaks found in the cyclic voltammogram of the material in Fig. 21 represent the insertion and rearrangement of lithium ions in both octahedral

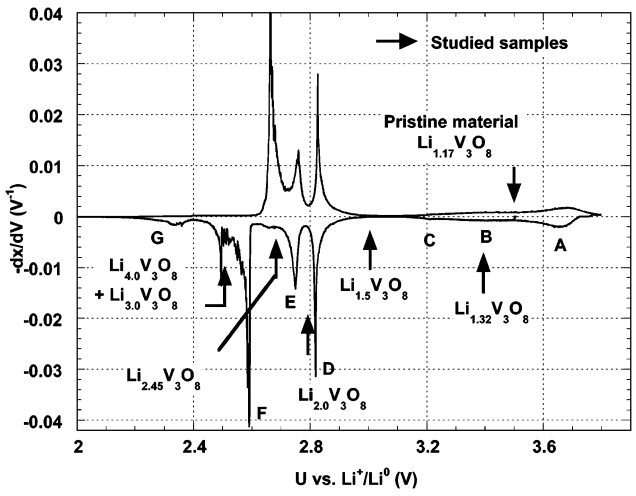

Fig. 21 Cyclic voltammogram obtained in potentiodynamic mode for the first cycle (the two first reductions and the first oxidation), between 3.8 and 2.0 V for $Li_{1+x}V_3O_8$ with a rate of 1.25 mV/h and a cutoff current corresponding to 1 Li/100 h. Reproduced with permission from N. Dupré, J. Gaubicher, D. Guyomard and C. P. Grey, *Chem. Mater.*, 2004, **16**, 2725–2733. Copyright The American Chemical Society 2004.

and tetrahedral sites in the structure, instead of their sequential filling, as has been suggested in theoretical studies.[153]

In several cases, the synthesis method has been found to affect the electrochemical properties of this material. Both Pistoia *et al.*[147] and West *et. al.*[148] showed that over four lithium per formula unit could be inserted into amorphous $Li_{1+x}V_3O_8$, while only three lithium were inserted in a crystalline sample prepared by improving the electronic conductivity through extrusion from the material. This is thought to be a consequence of the longer lithium diffusion path caused by the preference of the high-temperature material to cleave along a [001] plane as well as the flexible nature of the amorphous material. Brylev *et al.*[154] synthesized $Li_{1+x}V_3O_8$ through the thermal decomposition of various freeze-dried precursors and also found better electrochemistry for poorly-crystalline, small particle size materials.

Rozier *et al.*[155] found that the capacity of $Li_{1+x}V_3O_8$ decreased with increasing C rate, and attempted to lessen this phenomenon by improving conductivity through copper extrusion of the material $(Li_{01.3-y}Cu_y)V_3O_8$ during cycling. The loss of capacity was less in the copper-containing compounds than in $Li_{1.3}V_3O_8$; however the overall capacities and capacity retention were better for the $Li_{1+x}V_3O_8$ cells. Torardi and Miao[156] discussed the compound $M_{1-x}V_3O_{8-y}F_z \cdot nH_2O$ (where M = NH_4, K; $x \approx 0.0$–0.2; $y \approx 0.0$–0.2; $z \approx 0.1$–0.2; $n \approx 1$), which was synthesized by the precipitation in HF of ammonium and potassium vanadate solutions. The ammonium material was able to achieve a high initial discharge capacity of 400 mAh/g at a constant current of 0.36 mA/cm^2 but the capacity drops to 350 mAh/g on the second cycle. Forming a composite of the ammonium material with carbon in order to improve the electronic conductivity again resulted in a loss of capacity in the material.

The partially reduced compound $H_2V_3O_8$ [Fig. 19(b)] was first synthesized by Théobald and Cabala in 1970.[157] Its structure, closely related to that of $Li_{1+x}V_3O_8$ but with quadruple chains connected to double chains through the bridging oxygen, was determined by Oka *et al.*[158] The material can be chemically and electrochemically oxidized to form $Li_xH_{1-x}V_3O_8$, though it can only intercalate about 1.2 lithium per formula unit compared to 2.5 lithium in $H_2V_3O_8$ cells.[159,160] Highly flexible $H_2V_3O_8$ nanobelts, 100–500 nm wide, 10–50 nm thick and up to several hundred microns in length, can also be hydrothermally synthesized from a V_2O_5 precursor.[161] Initial capacity of these structures during cycling from 3.8 to 1.7 V at 30 mA/g is 253 mAh/g, which quickly falls to 235 mAh/g in the second cycle. Over the course of fifty cycles, a stable capacity of 229 mAh/g was reached. This value is higher than the capacity of approximately 190 mAh/g that has been determined for $H_2V_3O_8$ and $Li_xH_{1-x}V_3O_8$ of other morphologies,[40] due to the high surface area and shorter diffusion path for lithium in the nanostructure.

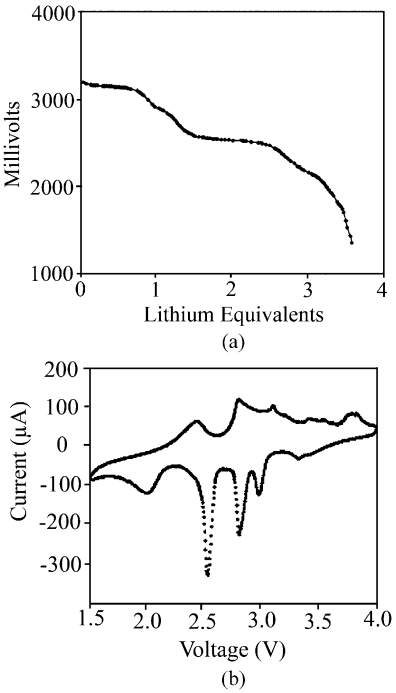

Fig. 22 Discharge voltage profile and slow rate voltammetry of silver vanadium oxide. Reproduced with permission from E. S. Takeuchi and W. C. Thiebolt, *J. Electrochem. Soc.*, 1988, **135**, 2691–2694. Copyright The Electrochemical Society 1988.

$Ag_xV_4O_{11}$ and related structures

Silver vanadium oxide (SVO) in the form of $Ag_2V_4O_{11}$ has been used extensively as a cathode material in primary lithium batteries for implantable medical devices, specifically in heart pace-makers and implantable cardiac defibrillators (ICDs). This device is able to correct a cardiac arrhythmia by releasing one or more electric pulses of various energies when it senses an irregularity in the heart's electric signals. SVO is an ideal cathode material for this purpose because it can produce the high current needed to give a high-energy pulse and has been tested extensively to prove that it is safe and reliable.[162] The distinct voltage profile [Fig. 22(a)] during the discharge of a Li/SVO cell allows doctors to determine the state of charge of the battery based on the voltage, making it easy to predict when the battery needs to be replaced. The batteries have a long shelf life and last around 10 years under lower current drain, with less than 2% self-discharge per year,[163] which is important for a battery that is used sporadically over the course of several years. Materials for this application do not need to have the excellent reversibility and capacity retention expected in other rechargeable batteries because they are replaced after one use.

The $Ag_2V_4O_{11}$ material was first reported in 1964[164] as one of several products of the reaction of Ag with V_2O_5 at various temperatures. It was also one of the phases seen in the study of the AgO_2–V_2O_5 system by Fleury *et al.* in 1966[165] and again in 1985 by Wenda.[166] An initial patent was issued in 1982, which disclosed the synthesis of several vanadium oxide–transition

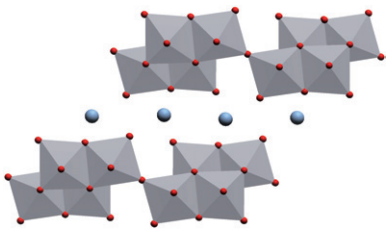

Fig. 23 Crystal structure of $Ag_2V_4O_{11}$.

metal composites, including $Ag_2V_4O_{11}$, by thermal decomposition and their subsequent use as cathodes in lithium batteries.[167] The SVO structure has a C-centered monoclinic unit cell consisting of layers of vanadium oxide with silver ions between them, as shown in Fig. 23. Vanadium atoms in the structure are in distorted octahedral coordination and form a layer in the [001] plane. The V_4O_{11} layers are built from quadruple V_4O_{12} chains along the *b*-axis, which share only one corner.[5] HREM and X-ray diffraction reveal lattice parameters of $a = 15.3$ Å, $b = 3.60$ Å, $c = 9.5$ Å, and $\beta = 128°$.[168]

Takeuchi and Thiebolt performed low scan rate voltammetry at 0.08 mV/s on the SVO cathode material to identify the five voltage plateaus in the discharge curve which correspond to five reductive processes taking place, as shown in Fig. 22.[169] From a comparison of this voltammetry with that of vanadium(V) oxide and silver oxide, it was determined that Ag was irreversibly reduced at a value of 2.6 V. Because SVO is its own unique structure and is not made up of a combination of vanadium and silver oxides, this technique can only show the potential values at which the metal centers are electrochemically active. However, Crespi *et al.* determined that Ag is reduced to silver metal and extruded from the lattice in the first reduction step in a polymer cell at 100 °C.[170] The reversibility of this reaction with about 45% capacity fading is supported by XRD of the cycled materials, while the appearance of Ag particles of 1–5 nm on the surface of the material before it has been cycled suggests that Ag reduction is the first step.[168] When the material is cycled at room temperature with an organic electrolyte, the reversibility is severely compromised and capacity fading is about 80% over 25 cycles. Tarascon and Garcia-Alvarado[171] found that the cycling of $Ag_2V_4O_{11}$ was reversible over the range of 3.6 to 1.5 V, intercalating up to 7 Li per formula unit while displacing Ag; however, reversibility suffered over the course of several cycles, and some Ag was eventually replaced irreversibly by about 2 Li. Kawakita *et al.*[172] showed that sodium ions stabilized the structure when they were used to substitute some of the silver ions in the compound $(Na_yAg_{1-y})_2V_4O_{11}$. Capacity fading was diminished compared to pure SVO due to a pillaring effect of the sodium ions that connects neighboring layers.

The compound $Cu_{2.33}V_4O_{11}$[173] has also been used as a cathode in lithium batteries despite the apparent lack of intercalation sites in its structure. Instead of a traditional intercalation reaction, a displacement reaction occurs where the Cu metal, in the form of micron-sized Cu dendrites, is continuously extruded from the structure at one end as it is being replaced by lithium ions at the other end (Fig. 24). The fully discharged state is amorphous; however, upon charging, the Cu goes back into the layers with no detrimental effect to the capacity or structure, and crystallinity is restored. The reversible insertion of 5.5 Li^+ leads to a stable capacity of approximately 250 mAh/g. The material is more rechargeable than SVO, but not sufficiently so for use in high rate applications. The related material, $Cu_{1.1}V_4O_{11}$, was synthesized through the partial removal of Cu from $Cu_{2.33}V_4O_{11}$ by electrochemical and chemical oxidation.[174] With a capacity of approximately 260 mAh/g, $Cu_{1.1}V_4O_{11}$ is similar to the parent compound except that not all of the Cu is removed during discharge, and the discharged structure is not amorphous.

Recently, SVO in the form $Ag_{0.35}V_2O_5$ has been formed into a flexible sheet of nanowires approximately 500 nm thick.[175] The wires themselves are 10–20 nm thick and have lengths on the millimeter scale. The *d* spacing was 10.7 Å and the wires grow along the [010] plane. These structures were used to make electrochromic devices with a red-brown oxidized state and a green reduced state. The short lithium diffusion distance and high conductivity in the SVO nanowires allowed short color change times of 0.2 s for green to red-brown and 0.1 s for the reverse process.

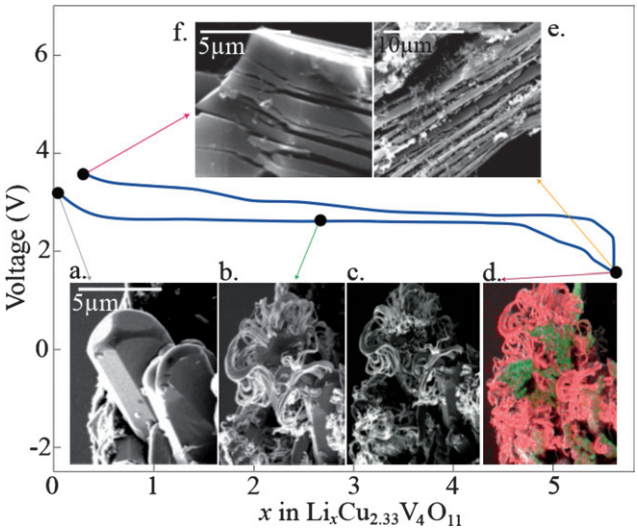

Fig. 24 Cu dendrites formed during cycling of $Cu_{2.33}V_4O_{11}$. Reproduced with permission from M. Morcrette, P. Rozier, L. Dupont, E. Mugnier, L. Sannier, J. Galy and J. M. Tarascon, *Nat. Mater.*, 2003, 2, 755–761. Copyright Nature Publishing Group 2003.

3. Vanadyl phosphates

Vanadium also forms a range of structures with the phosphate anion, several of which are layered. All these structures contain VO_6 octahedra, often highly distorted as in the oxides, and PO_4 tetrahedra. In the layered α-$VOPO_4 \cdot 2H_2O$ the oxygens in the basal plane of the VO_6 octahedra share corners with the PO_4 tetrahedra to form sheets, with one of the VO_6 apical oxygens forming a vanadyl bond, and the 6th position being barely occupied by a water molecule in the hydrates and by a long bond to a vanadyl oxygen in a neighboring layer for anhydrous material. This weak bonding leads to the ready intercalation of a number of electron donors, like imidazole, which can take up a number of configurations.[176] This layered structure loses its water in two steps, with the lattice spacing decreasing from 7.11 Å to 6.3 Å and finally to 4.11 Å in the dehydrated phase.[177] This layered structure can intercalate lithium reversibly, giving a capacity of 100 mAh/g for the hydrate, which corresponds to 0.8 Li/VPO_4; the theoretical capacity of the dihydrate is 135 mAh/g. However, the capacity decayed rapidly on cycling, due to the presence of the water molecules, which released oxygen gas on charging above 3.9 V. The fully dehydrated phases showed a much lower capacity of around 50 mAh/g, probably due to the low ionic conductivity, just as found for protonic conductivity in the anhydrous material.[178]

A comparative electrochemical study of anhydrous vanadyl phosphates, formed at elevated temperatures, has been made and

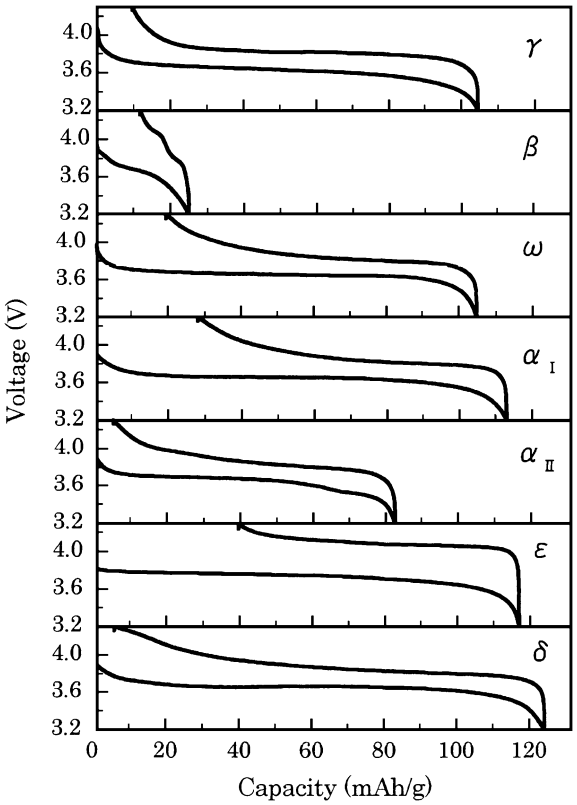

Fig. 25 Voltage profile as lithium is inserted into and removed from a series of vanadyl phosphates at 0.04 mA/cm^2 in the potential window of 3.2 to 4.3 V. Reproduced with permission from B. M. Azami, T. Ishihara, H. Nishiguchi and Y. Takita, *J. Power Sources*, 2003, **119–121**, 273–277. Copyright Elsevier 2003.

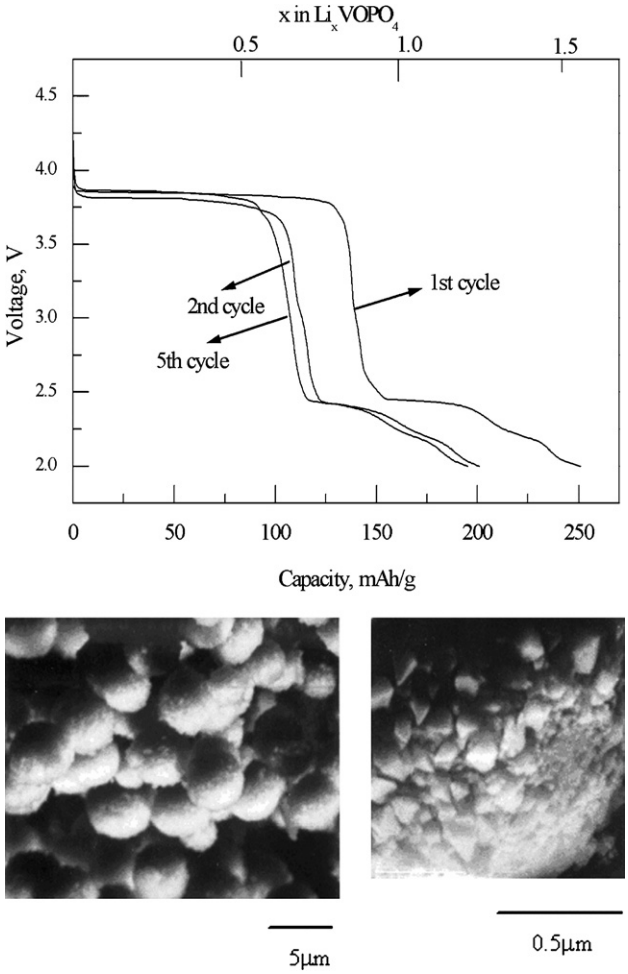

Fig. 26 (Top) Discharge curves of the Li/Li$_x$VOPO$_4$ cells cycled between 4.5 and 2.0 V in 1M LiPF$_6$-EC/DMC, 164 mAh/g = 1 Li), and (bottom) SEM of ε-VOPO$_4$ synthesized from tetragonal H$_2$VOPO$_4$, the inset shows a magnified view of one of the spherical particles. Reproduced with permission from Y. Song, P. Y. Zavalij and M. S. Whittingham, *J. Electrochem. Soc.*, 2005, **152**, A721–A728. Copyright The Electrochemical Society 2005.

the results are shown in Fig. 25.[179] The highest capacities are around 120 mAh/g, significantly lower than the theoretical capacity of 166 mAh/g for anhydrous VOPO$_4$ (excluding the lithium). Although the β-phase showed the lowest capacity, it has been found that if the β-LiVOPO$_4$ phase is formed carbothermally from the anhydrous VOPO$_4$ from the dihydrate, then the capacity is much improved at very low rates, for example 120 and 135 mAh/g at C/20 and C/40 rates respectively.[180]

Most of the above high temperature forms of vanadyl phosphate have a three-dimensional lattice, and the best capacities are much higher than that of the anhydrous layered VOPO$_4$ described above probably because the diffusion path is maintained at the correct size for lithium. One of the more interesting and more studied is the ε-VOPO$_4$ phase, which was first synthesized by the Jacobson group[181] by the dehydration of VOPO$_4$·H$_2$O at 550 °C: Its electrochemical behavior was reported[182] by the Nazar group shortly after its synthesis, with a value of 126 mAh/g at very low rates, around 75% of the theoretical capacity, but capacity fading was an issue. The structure of the intercalated product LiVOPO$_4$ is the same as that of high temperature LiVOPO$_4$.[182] This ready conversion from the VOPO$_4$·H$_2$O phase to the ε-phase then to the LiVOPO$_4$ phase suggests that all three have closely related structures. This was further emphasized when Song *et al.*[183] found that the protons in the VOPO$_4$·H$_2$O phase, which can also be written as H$_2$VOPO$_4$ could be removed either electrochemically or chemically at room temperature. The proton removal was found to be reversible: H$_2$VOPO$_4$ ↔ ε-VOPO$_4$. The protons were de-intercalated at a potential between 4.1 and 4.4 volts in a lithium-based non-aqueous cell giving ε-VOPO$_4$. On reversing the current lithium ions were inserted reversibly into the lattice forming LiVOPO$_4$ at about 3.8 V and Li$_2$VOPO$_4$ at 2.4 V, as indicated in Fig. 26. At a current density of 0.2 mA/cm^2, the capacity was almost 140 mAh/g (0.83 Li/VOPO$_4$) on the higher voltage plateau and reached 250 mAh/g when both plateaus are considered. However, there is a loss in capacity from the 1st to the 3rd discharge, but if cycling is restricted to above 3 volts then a steady capacity of 125 mAh/g is maintained. Even at 2 mA/cm^2 the extended capacity approaches 100 mAh/g for products made with the more disordered tetragonal H$_2$VOPO$_4$ precursor which is made-up of nanosized, around 50 nm, primary particles agglomerated into 3–5 μm spheres.

ε-VOPO$_4$ is not the only compound to react with more than one lithium per redox center. It is quite common in layered

materials, having being first reported in VSe_2[184] and subsequently in a number of layered oxides such as Li_2NiO_2[185] and $Li_2Ni_{0.5}Mn_{0.5}O_2$.[186] If a truly high energy density battery is to be developed with an intercalation-type mechanism, then materials such as these must be found that can maintain their structures on deep reaction. Presently in the layered compounds, the second lithium is incorporated in a two-phase system because to accommodate the extra lithium ions all the lithium ions must switch from octahedral sites to tetrahedral sites. An additional complication in vanadium oxide compounds is the ready mixing of the lithium and vanadium occupancies, resulting in disordered structures as observed for ω-$Li_3V_2O_5$, and possibly contributing to the loss of capacity of some of these vanadium phosphates by the locking-in of some of the lithium after cycling into non-accessible sites.

4. Molybdenum oxides

The most widely studied form of molybdenum trioxide is the stable layered orthorhombic structure usually referred to as the α-phase (or α-MoO_3), in which the basic structural unit is the MoO_6 octahedron. Unlike V_2O_5, this thermodynamically stable form of MoO_3 has a double sheet of MoO_6 octahedra, as shown in Fig. 27(a). As discussed earlier, the crystalline structure may be visualized as corner-sharing chains of MoO_6 octahedra that share edges with two similar chains to form layers of MoO_3 stoichiometry in the *ab*-plane. Within each MoO_6 octahedron one oxygen atom is essentially unshared forming a terminal Mo=O. The layers are stacked in a staggered arrangement along the *c* axis and are held together by van der Waals' forces. At least two metastable polymorphs of MoO_3 also exist. One of these, Fig. 27(b), has the same monoclinically distorted perovksite structure as WO_3, and is known as the β-phase.[187] The A position in this perovskite lattice, ABO_3, is vacant and can be the intercalation site for small cations such as protons and lithium ions just as in WO_3. A second metastable form of MoO_3 has the hexagonal lattice shown in Fig. 27(c); it has only been formed by

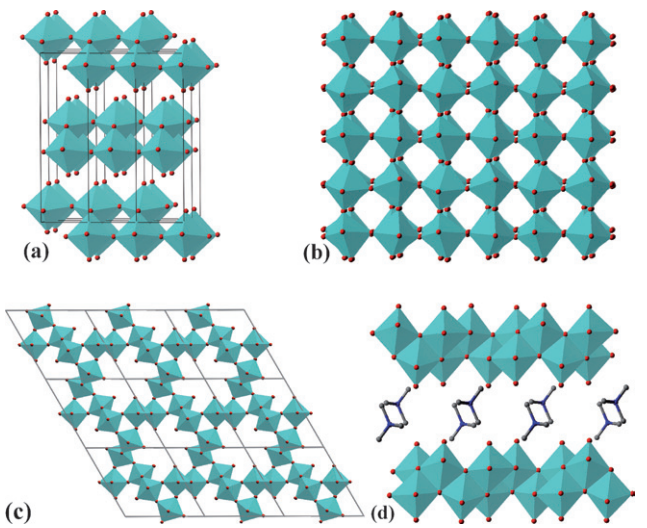

Fig. 27 Some structures of molybdenum trioxide: (a) stable layered α-MoO_3, (b) cubic β-MoO_3, (c) hexagonal h-MoO_3, and (d) layered $N(CH_3)_4HMo_4O_{12}$.

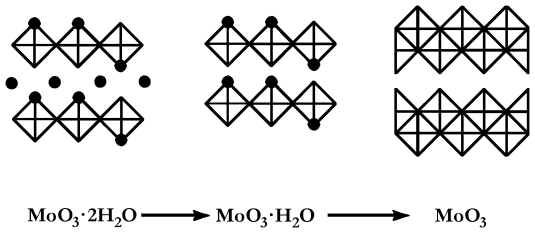

Fig. 28 The topotactic dehydration of molybdenum trioxide dihydrate, $MoO_3 \cdot 2H_2O$. The solid circles represent water. Reproduced with permission from M. S. Whittingham, *J. Electrochem. Soc.*, 1976, **123**, 315–320. Copyright The Electrochemical Society 1976.

the oxidative de-intercalation of the hydronium material, $(H_3O)_xMoO_3 \cdot nH_2O$.[188] The open crystal structures of these three molybdenum oxides enable the facile intercalation of lithium as well as other ions, and all three have been studied as battery cathodes. There are a number of other molybdenum trioxide compounds with layered structures. One of these is shown in Fig. 27(d), and it contains Mo_4O_{12} sheets between which reside organic cations, such as tetramethylammonium[189] in $(NCH_3)_4HMo_4O_{12}$ and ethylenediammonium[190] in $(C_2H_{10}N_2)Mo_4O_{12}$. Although these have a suitable structure for intercalation reactions, being layered and having tunnels in the sheets allowing ions to travel from one guest layer to the next, to date the organic ions have not been removed thus impeding lithium transport.

Although anhydrous MoO_3 contains double sheets of MoO_6 octahedra, single sheets are found in hydrated MoO_3 as indicated schematically in Fig. 28. The hydrates contain $MoO_5(H_2O)$ octahedra and in addition in $MoO \cdot 2H_2O$ intercalated water. On dehydration, the intercalated water is lost first, then neighboring sheets condense giving the double sheets as the final water is lost. The lithium intercalation properties of hydrated MoO_3 will be described below.

MoO_3 for Li-ion battery electrodes

Molybdenum oxide was proposed in the 1970s as a cathode material for Li-ion batteries,[191–193] and a typical discharge curve is shown in Fig. 29. In an early report, a comparative study of amorphous versus crystalline MoO_3 showed that the crystalline material had a higher and flatter voltage profile versus Li^+/Li for different degrees of Li insertion up to ~1.6 Li^+/MoO_3.[194] It was also shown that polycrystalline MoO_3 undergoes significant degradation with lithium insertion of 1.5 Li^+/MoO_3 resulting in a loss of electronic conductivity in the molybdenum oxide cathode.[195] Discharge capacities that were approximately twice as high as that observed for MoO_3 were observed for molybdenum oxide hydrates, but the recharge efficiencies never exceeded 50%.[196] Studies of substoichiometric molybdenum oxides indicated that Mo_8O_{23}[197] and $Mo_{17}O_{47}$[198] could have superior properties to MoO_3. However, similar to all of the early studies, the oxygen deficient structures were limited by low recharge efficiency and poor cycling stability.

The electrochemical properties of disordered and crystalline MoO_3 have also been extensively probed more recently. In 1994 Julien *et al.* performed an in-depth study of crystalline α-phase MoO_3 and polycrystalline thin films for cathode applications.[199]

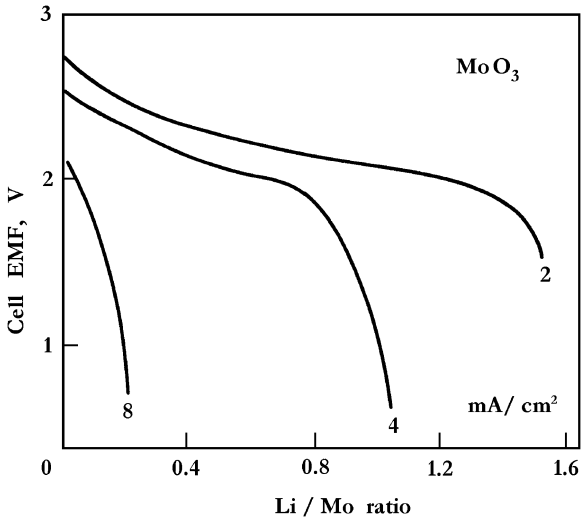

Fig. 29 Discharge behavior of crystalline MoO_3 at 2, 4 and 8 mA/cm^2.[13] Reproduced with permission from M. S. Whittingham, *Progress in Solid State Chemistry*, 1978, **12**, 41–99. Copyright Elsevier 1978.

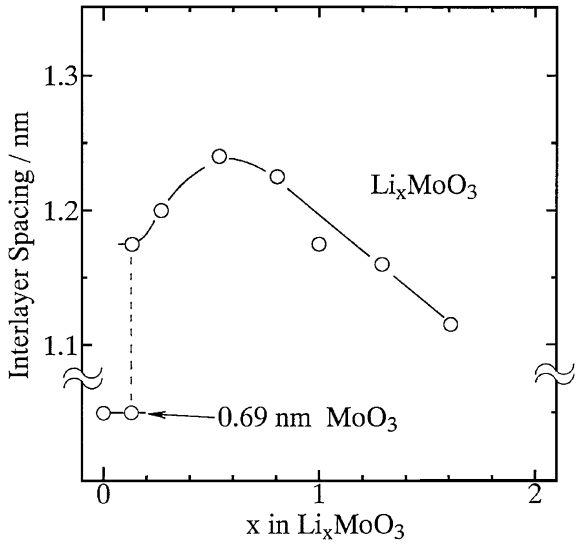

Fig. 30 Change in interlayer spacing between Mo–O octahedron layers of Li_xMoO_3 with lithium composition. Reproduced with permission from T. Tsumura and M. Inagaki, *Solid State Ionics*, 1997, **104**, 183–189. Copyright Elsevier 1997.

In that study it was found that the kinetically accessible discharge range was $0 \leq x \leq 1.5$ in Li_xMoO_3 and that the operating potential for the disordered phases was higher than that of the crystalline. The open circuit potentials ranged from 3.2–2.5 V, and the cells were discharged to 1.5 V versus Li^+/Li. The chemical diffusion coefficient of the crystalline film was found to be 10^{-9} cm^2/s for $x = 0.7$ and ranged from 10^{-11}–10^{-12} cm^2/s for disordered polycrystalline films with a thermodynamic factor that was approximately two orders of magnitude higher than in MoO_3 crystals.[199] It was speculated that when long-range order is reduced, the presence of small crystallites reduces the probability that diffusing ions impinge on a channel in the MoO_3 host structure and that the site energies and densities are not the same.[200] The ionic conductivity of the MoO_3 crystals was also shown to increase with increasing Li-insertion reaching a maximum value of 1.5×10^4 S cm^{-1} for $x = 0.7$ in Li_xMoO_3.[201]

The changes in the interlayer spacing of crystalline MoO_3 samples was extensively studied with cut-off voltages of 3.4–1.5 V versus Li^+/Li. Because of the large distortion that occurred during Li insertion, a variety of samples with different degrees of crystallinity were shown to have similar electrochemical performance. The distortion that occurs with lithium intercalation results in the gradual formation of a new Li_xMoO_3 phase which coexists with the MoO_3 phase until $x \sim 0.25$.[202–204] For $0.25 \leq x \leq 1.6$ only a Li_xMoO_3 phase is observed. The initial formation of the lithiated phase results in expansion of the interlayer spacing from 0.69 nm to 1.175 nm. As shown in Fig. 30, the interlayer spacing of the lithiated MoO_3 phase then widens from 1.175 to 1.24 nm but finally shrinks to 1.115 nm as 1.6 Li are inserted per MoO_3. It was speculated that the shrinkage was due to an increase of Coulomb interactions between solvated lithium ions and the host caused by the increase in packing density of the inserted species.[202]

The hexagonal phase of MoO_3 readily intercalates lithium up to about 1.5 Li/Mo, as indicated in Fig. 31 for the empty tunnel structure and for one containing silver, $Ag_{0.2}MoO_3$.[188] Fig. 31 also shows that up to ~ 2 Li^+/Mo could be inserted into

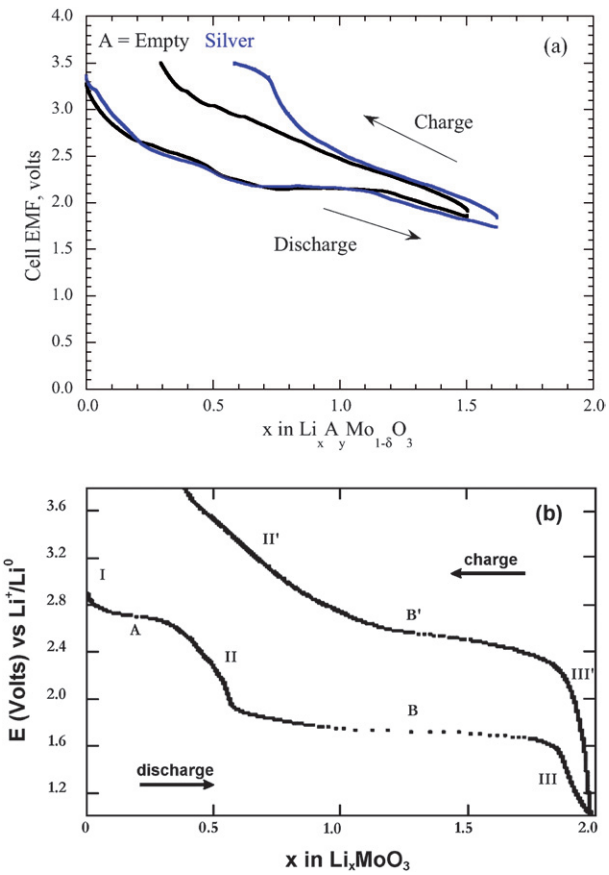

Fig. 31 Electrochemical cycling curve of (a) hexagonal MoO_3 and (b) β-MoO_3, showing the different structural regions, I, II and III being single phase regions, and A and B two-phase regions. Reproduced with permission from (a) J.-D. Guo, P. Zavalij, and M. S. Whittingham, *J. Solid State Chem.*, 1995, **117**, 323, and (b) I. J. Ramirez and A. Martinez del la Cruz, *Materials Letters*, 2003, **57**, 1034–1039. Copyright Elsevier 1995 and 2003.

metastable crystalline β-phase MoO_3, on discharge between 3.2–1.1 V versus Li^+/Li, with the value decreasing by 25% after the first cycle and significant capacity fade occurring in only five cycles. In the first insertion the structure proceeded from the cubic phase through rhombohedral phases to an amorphous phase upon complete insertion of 2 Li^+.[205]

Li insertion in hydrated molybdenum oxides has also been studied for Li-ion cathode applications in more recent investigations. An ionic resin exchange technique was employed for the formation of polycrystalline $MoO_3 \cdot (1/2)H_2O$ and amorphous $MoO_3 \cdot 1H_2O$. The diffusion coefficient for the polycrystalline $MoO_3 \cdot (1/2)H_2O$ was found to vary from $\sim 3 \times 10^{-8}$ to 3×10^{-9} cm^2/s as the number of inserted lithium increased from 0.05 to 1.5. However, for the amorphous $MoO_3 \cdot 1H_2O$, the diffusion coefficient remained fairly constant with Li insertion at the higher value of 3×10^{-8} cm^2/s. The drop in the diffusion coefficient for the $MoO_3 \cdot (1/2)H_2O$ was attributed to interfacial blocking in the polycrystalline material.[206] In a different study the diffusion coefficient of $MoO_3 \cdot (2/3)H_2O$ was shown to peak at $\sim 5 \times 10^{-9}$ cm^2/s with approximately 0.7 Li^+/MoO_3.[207] Electrochemical lithium insertion in amorphous $MoO_3 \cdot 2H_2O$ was shown to surpass that of both anhydrous MoO_3 and other hydrated molybdenum oxides with an initial capacity of 3.3 Li^+/MoO_3 or 400 mAh/g. However, only 55% of the lithium was removed reversibly in the first cycle. The irreversible insertion was similar to that observed previously[196] and was attributed to a possible irreversible reaction between the inserted Li and the coordinated water in the hydrate host. It was also shown that after 30 electrochemical cycles the reversible capacity decreased to 1 Li^+/MoO_3.[208]

Various routes to modify MoO_3 in an effort to improve the cycling stability have also been explored. For example, Sn-treated MoO_3 cathodes were fabricated by the reaction of water-free tin dichloride with fine particulate orthorhombic MoO_3. The tin-reduced samples still retained the crystalline α-phase MoO_3 structure and were shown to have significantly improved cycling capabilities compared to a non-treated reference MoO_3 sample. Cycling at ~C/10, the discharge capacity of the tin-reduced samples was over 100 mAh/g after 20 cycles while the capacity of the MoO_3 sample was reduced to 45 mAh/g. After 100 cycles the Sn-treated MoO_3 capacity stabilized at close to 100 mAh/g. The improved performance was attributed to either improved conductivity from the tin coating and/or improved mechanical properties due to amorphization during the reduction process.[209] The effects of Pt nanoparticle incorporation into a MoO_3 thin film have also been studied. The films were produced by co-sputtering Pt and MoO_3 to obtain ~1.5 nm sized Pt particles in a bed of MoO_3. Improved cycling performance was observed for the Pt-doped films as a stable capacity of ~120 mAh/g was observed for 30 cycles at ~C/10. It was shown that the film containing Pt particles both had a higher conductivity and did not experience as much structural degradation during cycling.[210] Chemical lithiation of α-MoO_3 was also shown to improve the cycling performance. In general the Li_xMoO_3 species with $x = 0.1, 0.25, 0.5, 1$ showed marked improvement in cycling performance compared to nonlithiated MoO_3, retaining a capacity of ~65 mAh/g after 30 cycles at ~C/8 with the MoO_3 electrode fading to a capacity less than that in only 20 cycles. The lithiated samples were also shown to have improved electronic conductivity.[211] Finally $Na_{0.25}MO_3$ was explored as a potential Li-ion anode material with the samples prepared by a simple reduction of MoO_3 in the presence of Na_2MoO_4. Sodium-doped molybdenum oxide was shown to have a high initial capacity of 940 mAh/g when cycled in a voltage window of 3.0–0.005 V, but the capacity degraded to 400 mAh/g in ~100 cycles.[212] By increasing the cut-off potential to 0.2 V and employing a slow rate (discharge and charge at C/15 and C/20, respectively), the cycling was more stable, ranging from 600 mAh/g–400 mAh/g in 100 cycles.[212] A tin-doped MoO_3 system was also explored as an anode, and the average charge potential was lowered, but at the expense of capacity fading.[213]

Various micro- and nanostructures of α-MoO_3 have also been recently studied in order to improve the cycling stability of Li-ion electrodes. Molybdenum oxide microrods with diameters of ~2–6 μm were formed at high density with a simple vapor transport process. The microrods were investigated for their properties as a cathode and were compared to ball-milled MoO_3 particles. When cycled in a voltage window of 3.25–2.0 V versus Li^+/Li at ~C/4, the microrods retained a reversible capacity of 199 mAh/g which was 88.4% of the highest capacity while the particle electrode exhibited a capacity of only 85 mAh/g after 100 cycles corresponding to 47.2% of the initial capacity. It was speculated that the rod-like structures could more easily accommodate the structural strain that occurred upon Li insertion.[214] The electrochemical properties of α-MoO_3 nanorods have also been explored for improved cathode applications. A high initial capacity of 255 mAh/g was observed for the nanorods compared to bulk material that had an initial capacity of 201 mAh/g. Upon cycling the nanorods appeared to have a fairly stable capacity of ~130 mAh/g after 10 cycles with the bulk decreasing to ~63 mAh/g.[215] α-MoO_3 nanobelts synthesized by a hydrothermal method with widths of 80–400 nm and lengths of 5–10 μm were also studied as potential cathode materials. The nanobelts had an initial capacity of ~300 mAh/g, but it was decreased to only 180 mAh/g in 15 cycles at C/10. The cycling stability was improved by prelithiating the nanobelts with LiCl. The initial capacity was reduced to 240 mAh/g but shown to be 220 mA/g after 15 cycles (92% capacity retention).[216]

The recent interest in oxides, and in particular nano-oxides,[4] for anodes for HEV lithium batteries is driven by the desire for an anode with a slightly more positive insertion voltage with respect to Li^+/Li to minimize any risks of high-surface-area Li plating while charging at high rates, a major safety concern.[217] In hybrid electric vehicles, batteries are cycled with ~10% charge/discharge from the point where the cell is at 50% capacity.[218] Thus the ideal negative electrode for forthcoming vehicular applications may have a charge/discharge potential of ~0.5 V vs. Li^+/Li when it is approximately one-half charged. The state-of-the-art graphite anode operates at a potential of 0.1 V relative to Li^+/Li. Consequently, MoO_3 and other transition metal oxides[219–222] that operate at higher potential than graphite are under consideration for next generation anode technologies.

Recently, α-phase MoO_3 nanoparticles with diameters of 5–20 nm have been produced by hotwire chemical vapor deposition, as previously used for WO_3.[223] These have been examined as a new anode material as it is possible to insert more than ~1.5 Li^+/MoO_3 into the molybdenum oxide matrix by reducing the potential closer to that of lithium metal during discharge. For

example, a thin film MoO_3 nanoparticle electrode (~2 μm thick) was shown to have a reversible capacity of ~630 mAh/g corresponding to the reversible insertion of ~3.4 Li/MoO_3. Furthermore, the nanoparticle anode showed no capacity degradation for 150 cycles between 3.5 to 0.005 V with both charge and discharge at C/2. Under identical conditions micron-sized particles were shown to quickly degrade as shown in Fig. 32. Upon cycling, long-range order in the MoO_3 nanostructures was shown to be lost due to a significant volume expansion upon lithium insertion. This volume expansion makes the failure of bulk MoO_3 and even large particles not surprising. The stability of nanoparticles stems from two possible mechanisms to limit stress, one being that the small size limits the maximum lithium concentration gradient that can develop, and the other that the surface is unconstrained in the normal direction, thereby providing stress reduction in the vicinity of the surface, which for nanoparticles encompasses most if not all of the particle. In larger MoO_3 particles where fracturing will result due to expansion/contraction, degradation will occur due to a loss in conductivity.[224] More recently, the MoO_3 nanoparticles have been fashioned into thicker electrodes (~100 μm) with a conductive additive and binder and tested in a coin cell configuration. The first two charge/discharge cycles for an electrode made of 70 : 10 : 20 MoO_3 nanoparticles : acetylene black : polyvinylidene fluoride are shown in Fig. 32. In the first cycle, the capacity of ~1230 mAh/g corresponds to a total of ~6.6 Li^+/MoO_3 inserted across this voltage range. The value of 6.6 Li^+/MoO_3 exceeds the maximum expected value of 6 Li^+/MoO_3. The extra capacity observed in the first discharge for the MoO_3 nanoparticles is most likely due to a side reaction with the electrolyte, as observed for other metal producing oxides.[4] In the second cycle, the quantity of inserted lithium is reduced to ~5.5 Li^+/MoO_3 with a capacity of ~1020 mAh/g. In subsequent cycles a stable capacity of ~850 mAh/g is achieved, corresponding to ~4.6 Li/MoO_3. The increased capacity for the MoO_3 coin cell electrode compared to the thin film electrode may be attributed to improved electronic/ionic mobility with the conductive additive and more complete accessibility to the nanostructures.

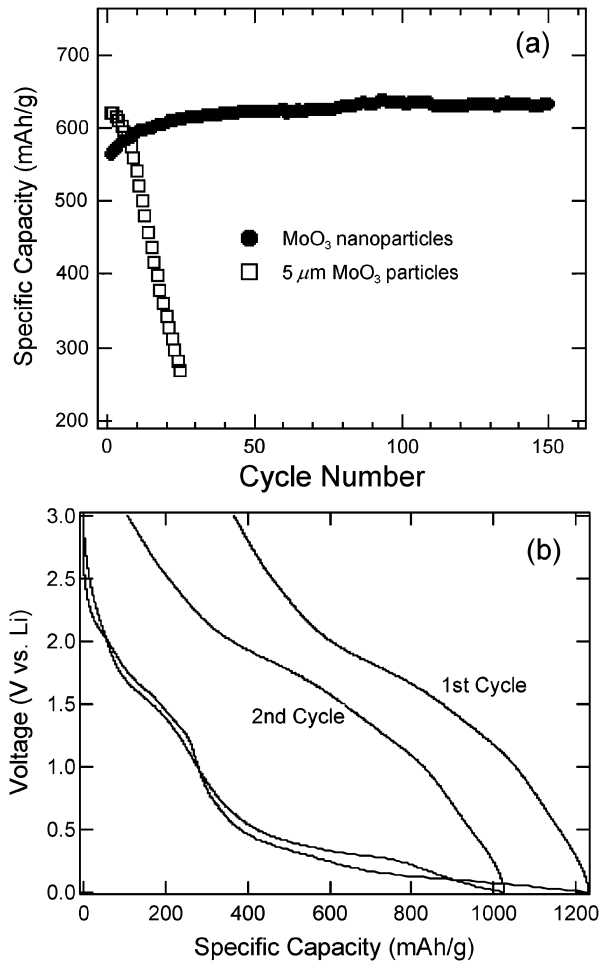

Fig. 32 (a) The cycling stability of an MoO_3 nanoparticle thin film electrode compared to commercially available μm-sized MoO_3 particles and (b) charge/discharge curves of the 1st and 2nd cycles for an electrode made of 70 : 10 : 20 MoO_3 nanoparticles : acetylene black : polyvinylidene fluoride tested in a coin cell configuration. (b) Reproduced with permission from S.-H. Lee, Y.-H. Kim, R. Deshpande, P. A. Parilla, E. Whitney, D. T. Gillaspie, K. M. Jones, A. H. Mahan, S. B. Zhang and A. C. Dillon, *Adv. Mat.*, 2008, **20**, 3627–3632.

MoO_3 electrochromic properties

The electrochromic (EC) effect, which occurs for many transition metal oxide materials, was recognized by Deb in 1969.[3] Electrochromism may be defined as transmittance modulation that reversibly occurs by electrically controlling the oxidation states of the transition metal. Operation of conventional EC devices is dependent upon reversible electrochemical double injection of positive ions (H^+, Li^+, Na^+, K^+) and electrons into the host lattice of multivalent transition metal oxide materials.[225,226] Both WO_3 and MoO_3 are well-known electrochromic materials that show cathodic coloration with electron injection and charge-balancing ion insertion. Alternately, some electrochromic materials color anodically by the removal of electrons and positive ions.[227] The most frequently studied materials with anodic coloration are NiO_2 and IrO_2. By combining an electrode that exhibits cathodic coloration with a counter electrode that has anodic coloration, it is possible to fabricate a more efficient and visually appealing EC device. Electrochromic films are being developed for application in dynamic or "smart" window technologies that are at the forefront of emerging energy saving advances in building technologies.[228,229] These dynamic windows may be darkened or lightened electronically with small voltages allowing for control of daylight, solar heat gain, and internal heat loss through windows of buildings and vehicles. The electrochromic effect may also be employed for sensors[230] and displays.[231] However, for display applications significant improvement in durable switching rate must be achieved.[232]

Coloration efficiency (CE) is one of the most important metrics for selecting an electrochromic material and is defined as the change in optical density (OD) per unit inserted charge (Q), *i.e.* $CE = \Delta(OD)/\Delta Q$. A high CE provides large optical modulation with small charge insertion or extraction. This is a crucial parameter for EC devices since a lower charge insertion or extraction rate enhances long-term cycling stability, another critical property. Substoichiometric WO_3 films have been shown to have the highest CE over the visible region and also have fast

response time and long lifetimes.[233–235] Tungsten oxides have therefore been the most extensively studied inorganic EC materials. Substoichiometric MoO_3 films also show pronounced electrochromism with behavior that is quite similar to tungsten oxide.[236,237] Although the coloration efficiency and cycle life of MoO_3 films are inferior to those of WO_3, the colored state of the molybdenum bronze is better matched to the sensitivity of the human eye.[238] It also absorbs light more intensely and more uniformly in the visible range.[227] As-deposited molybdenum oxide films are transparent, but when ions such as H^+ or Li^+ and electrons are injected, the color of the films changes to dark blue. Similar to WO_3, the absorptive optical change in the films has been correlated directly to the injection/extraction of electrons and ions in the films and can be written in a simplified form as:

$$xM^+ + xe^- + MoO_3 \leftrightarrow M_xMoO_3\ (M = Li^+, H^+, Na^+)$$

For disordered MoO_3 materials the coloration mechanism is related to the reversible character of the redox process between the two oxidation states, *i.e.* electron exchange between adjacent Mo^{5+} and Mo^{6+} ions.[239] Reversible coloration occurs upon cathodic reduction of the molybdenum, and bleaching occurs with anodic oxidation. Similar to WO_3, disordered MoO_3 materials generally exhibit better coloration efficiency and reversibility than bulk crystalline materials.[236,240] For crystalline materials a different mechanism is believed to be operative, and the model to explain the electrochromism has been centered on free electron effects. Upon ion/electron insertion, the crystalline material can be viewed as having a variable electron density with electrons undergoing scattering predominantly against the intercalated ions. The optical properties can then be understood schematically by Drude theory and in more detail by Gerlach's theory.[227] The electrochromic effect has been extensively probed for amorphous MoO_3 films. A significant body of research on electrochromism for disordered partially crystalline or polycrystalline materials has also been performed. However, nanocrystalline MoO_3 materials for EC applications have been studied, to date, only briefly.

In several cases rf sputtering has been employed to show the effect of oxygen deficiency on the electrochromic properties of amorphous MoO_3 films. For example, in a 1985 study of sputtered MoO_3, it was found that films prepared in an atmosphere containing low partial pressures of oxygen had superior electrochromic properties to those formed in a high oxygen partial pressure.[241] For MoO_3 films formed in Ar with 0.5–5% O_2, a linear change in the optical density of the films was observed for charge injection up to ~50 mC/cm^2 resulting in deep blue coloration. Conversely, the films deposited in Ar with 30–50% O_2 could not be colored blue electrochemically, and a nonlinear relation between optical density and injected charge was observed for the initial coloration stage. A coloration efficiency of ~20 cm^2/C (500 nm) was observed for the films deposited with a lower oxygen concentration.[241] A subsequent study also confirmed that the highest electrochemical transmittance change is observed for sputter-deposited MoO_3 amorphous films that are oxygen deficient.[242] Finally, the effect of MoO_3 stoichiometry on electrochromic properties was recently demonstrated when films were again produced by sputtering a molybdenum target in an O_2·Ar ambient, and the oxygen flux was varied.[243] The highest transmission change $\Delta T = 35\%$ was observed for lower oxygen flux, resulting in the formation of a substoichiometric amorphous film. A charge insertion of 100 mC/cm^2 was observed corresponding to $x = 2.5$ for Li_xMoO_3, compared to $x = 1.5$ for crystalline stoichiometric MoO_3 films.[199] The electrochromic efficiency of the disordered, substoichiometric MoO_3 films was 16 cm^2/C (632.8 nm).[243]

In 1984 a new electrochemical method was demonstrated for the deposition of an electrochromic MoO_3 thin film on indium tin oxide (ITO) glass. The ITO glass was cathodically electrolyzed in an aqueous solution containing lithium molybdate, resulting in an oxide film with reversible electrochromic properties. Furthermore, a high electrochromic efficiency of ~45 cm^2/C (600 nm) was achieved.[244] More recently, very smooth amorphous $MoO_3 \cdot nH_2O$ films were fabricated by a simple spin coating technique employing a solution of peroxo-polymolybdic acid formed from the direct reaction of metallic molybdenum with hydrogen peroxide. Upon heating the film to temperatures between 80–150 °C, reversible electrochromism was again observed.[245] In 2000 Zhang *et al.* employed a sol-gel process to show that the electrochemical reversibility was dramatically improved for prefabricated Li-doped MoO_3 films. The Li-doped MoO_3 films were prepared using a lithium doped peroxo-polymolybdate precursor solution. For comparison the same technique was employed to fashion MoO_3 films in the absence of lithium. Amorphous films were obtained by annealing the as-prepared films for 1 hour at 120 °C. Fig. 33(a) shows cyclic voltammograms of the pure MoO_3 film at a sweep rate of

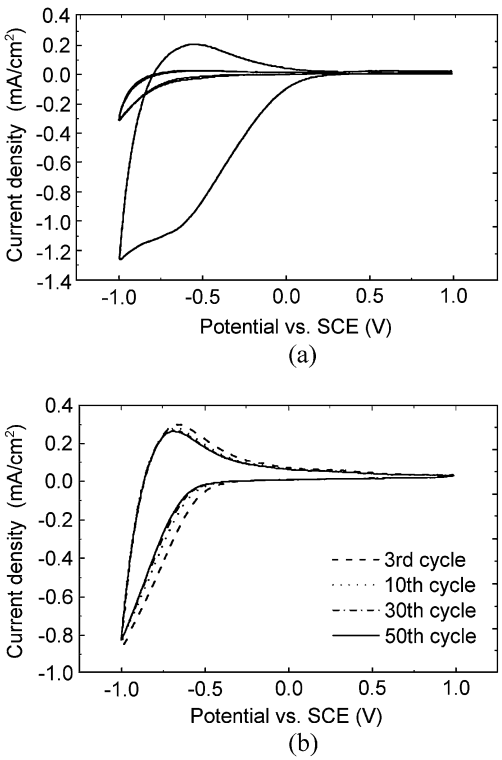

Fig. 33 Cyclic voltammograms of sol-gel prepared films heated to 120 °C for 1 hr for (a) amorphous MoO_3 and (b) Li-doped MoO_3. Reproduced with permission from Y. Zhang, S. Kuai, Z. Wang and X. Hu, *Appl. Surf. Sci.*, 2000, **165**, 56–59. Copyright Elsevier 2000.

20 mV/s from −1.0 to +1.0 V vs. SCE in 1 M $LiClO_4$/propylene carbonate (PC). Only two cycles are shown as significant irreversible insertion occurs in the first cycle with subsequent degradation in the second cycle. In contrast, Fig. 33(b) shows cyclic voltammograms of the Li-doped MoO_3 films obtained at a higher sweep rate of 50 mV/s. Some degradation is observed between the third and the tenth cycle but a pronounced improvement in durability is achieved. The initial degradation in reversibility was determined by analyzing the injected and extracted charge, and it was shown that 83.5% of the injected charge was extracted from the film in the 10th anodic half cycle, after which good reversibility was obtained. A relatively low transmission change $\Delta T = 35\%$ at 630 nm and a coloration efficiency of 7.86 cm^2/C were observed for the Li-doped films that exhibited the enhanced durability.[246]

Amorphous molybdenum oxide films deposited with electron beam evaporation have also been shown to be suitable for electrochromic applications as a significant change in absorption was observed when the films were doped with Li_2O.[247] In a more detailed study, electron beam evaporation was employed to carefully study the electrochromic properties versus substrate deposition and post-annealing treatments. The films produced at room temperature that were not annealed exhibited the best electrochromic properties with coloration efficiencies of 30 and 35 cm^2/C at 633 and 1033 nm, respectively. The room temperature deposited film was amorphous,[248] and the improved EC performance was attributed to the disorder in the films.[249] Vacuum evaporation has been employed to show that an increase in coloring and bleaching current densities may be achieved by evaporating a thin Au (20 nm) film on amorphous MoO_3. The effect is attributed to electrocatalytic properties of the thin gold layer.[250]

Electrochromism has also been studied for partially crystalline or polycrystalline MoO_3 films. In 1988 chemical vapor deposition was employed for the fabrication of MoO_3 polycrystalline thin films with a $Mo(CO)_6$ precursor. A high coloration efficiency of 51 cm^2/C was achieved at 633 nm.[251] Later, polycrystalline molybdenum oxide was prepared from the oxidation of molydenum trisulfide films followed by subsequent annealing to 400 and 550 °C. A plate-like structure was observed with the plates increasing in size with increasing annealing temperature. The films heated to 400 and 550 °C had coloration efficiencies of 30 and 10 cm^2/C (632.4), respectively, with decreased performance at the higher temperature attributed to a higher degree of crystallization.[252] In 1995, an improvement in the electrochromic effect for polycrystalline MoO_3 films was reported for films fabricated with an electrodeposition process.[253] The as-deposited films exhibited X-ray diffraction peaks indicative of the metastable tetragonal $MoO_{2.8}$ phase. Upon annealing to 260 °C, the films were transformed to a partially crystalline stable α-phase, and complete crystallization was observed following annealing to 300 °C. The heat treatment was shown to affect the reversibility of the electrochromic coloration. For the as-deposited films poor reversibility was observed with cyclic voltammetry. After 30 cycles the charge insertion decreased from 64.2 mC/cm^2 to 29.2 mC/cm^2 resulting in a permanent light blue coloration of the film. For the partially crystalline film, heat-treated to 260 °C, the reversibility was clearly improved. However, some capacity degradation was still observed after 25 cycles with significant degradation occurring in 100 cycles. Films heat-treated to higher temperatures exhibited pronounced degradation in the reversible electrochromism. The maximum value for the coloration efficiency was 41 cm^2/C at 700 nm for the films heated to 260 °C.[253]

More recently, MoO_3 films were prepared with cathodic electrodeposition from aqueous peroxy-polymolybdate followed by sintering at temperatures between 25–450 °C.[254] The films heat-treated at 100 °C or less were amorphous whereas those heated to 250 °C were a disordered mixed phase material comprised of both α- and β-MoO_3. Crystallization to α-MoO_3 occurred for temperatures above 350 °C. For the disordered polycrystalline phase obtained at 250 °C, the coloration efficiency was observed to improve to 15.8 cm^2/C compared to 6.3 cm^2/C (633 nm) for the amorphous film. However, the reversible cycling in 1M $LiClO_4$/PC was shown to decrease for the polycrystalline case. In the second cycle the reversibility for the polycrystalline film was only 67.2% compared to 93.4% for the amorphous material.[254] It has also been reported that the cycling stability of polycrystalline materials is improved upon cycling in 0.1 M $LiClO_4$, 14 mM $HClO_4$, 2% H_2O/PC rather than in a pure nonaqueous electrolyte, 0.1 M $LiClO_4$/PC. In this study a coloration efficiency of 35 cm^2/C was reported at 634 nm.

Although nanocrystalline species are likely present in the polycrystalline materials, very few studies have directly reported on the electrochromic effect on MoO_3 nanoparticles. In 2003 an electrochromic response was observed for nano-MoO_3 (~3–4 nm particles) encapsulated in mesoporous silicon. It was not possible to determine the extent of MoO_3 crystallization with wide-angle X-ray diffraction due to the silica background. However, when the samples were impregnated with hydrazinium sulfate as a reducing agent, a coloration change to blue was observed.[255] A very recent study employed electrochemical methods to directly demonstrate the electrochromic properties of nanocrystalline MoO_3 thin films prepared by a sol-gel spin coating technique and subsequent annealing to temperatures between 100–500 °C. Fig. 34 displays a SEM micrograph of the nanocrystalline nature of a film annealed to 350 °C that exhibited the best electrochromic properties.[256] For this film a coloration efficiency of 38.6 cm^2/C was observed at 700 nm. Importantly, minimal degradation was observed with cyclic voltammetry in

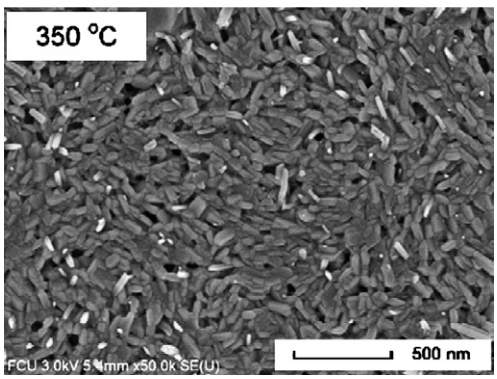

Fig. 34 SEM micrograph of nanocrystalline MoO_3 film. Reproduced with permission from C.S. Hsu, C. C. Chan, H. T. Huang, C. H. Peng and W. C. Hsu, *Thin Solid Films*, 2008, **516**, 4839–4844. Copyright Elsevier 2007.

1 M $LiClO_4$/PC after 100 cycles. Thus for the nanocrystalline material a comparable coloration efficiency to the best amorphous and polycrystalline films is observed with improved cycling stability.[253] The improved reversibility at the nanoscale is similar to that reported for nanoparticle MoO_3 Li-ion battery electrodes.[224]

5. Conclusions

There is much intriguing chemistry still remaining to be able to fully understand the structures of vanadium oxides and how to stabilize them, so as to exploit their very high reactivity with lithium and other intercalating cations. In the case of molybdenum oxide, very little is known about their layered structures apart from MoO_3 itself, and even there the opportunities of nano-MoO_3 are only now being uncovered.

Acknowledgements

We thank the National Science Foundation, through grant DMR-0705657, and the U.S. Department of Energy, through the BATT program at LBNL, for support of the work at Binghamton. A. C. Dillon would like to thank Leah Riley of NREL for supplying figures. The NREL work was funded by the U.S. Department of Energy under subcontract number DE-AC36-08GO28308 through: DOE Office of Energy Efficiency and Renewable Energy Office of the Vehicle Technologies Program and the Office of Building Technologies Program.

References

1 P. G. Dickens and M. S. Whittingham, *Quart. Rev. Chem. Soc.*, 1968, **22**, 30.
2 P. G. Dickens, R. M. P. Quilliam and M. S. Whittingham, *Mater. Res. Bull.*, 1968, **3**, 941.
3 S. K. Deb, *Appl. Opt. Suppl.*, 1969, **3**, 192.
4 M. S. Whittingham, *Dalton Trans.*, 2008, 5425.
5 P. Y. Zavalij and M. S. Whittingham, *Acta Cryst.*, 1999, **B55**, 627.
6 T. Chirayil, P. Zavalij and M. S. Whittingham, *J. Electrochem. Soc.*, 1996, **143**, L193.
7 T. A. Chirayil, P. Y. Zavalij and M. S. Whittingham, *Chem. Mater.*, 1998, **10**, 2629.
8 M. Greenblatt, *Chem. Rev.*, 1988, **88**, 31.
9 M. S. Whittingham and R. A. Huggins, *J. Chem. Phys.*, 1971, **54**, 414.
10 M. S. Whittingham, *J. Electrochem. Soc.*, 1976, **123**, 315.
11 C. R. Walk and J. S. Gore, *J. Electrochem. Soc.*, 1975, **122**, 68C.
12 C. R. Walk and N. Margalit, *J. Power Sources*, 1997, **68**, 723.
13 F. W. Dampier, *J. Electrochem. Soc.*, 1974, **121**, 656.
14 M. Broussely, P. Biensan and B. Simon, *Electrochimica Acta*, 1999, **45**, 3.
15 J. M. Tarascon and M. Armand, *Nature*, 2001, **414**, 359.
16 M. S. Whittingham, *Chemical Reviews*, 2004, **104**, 4271.
17 L. Kihlborg, *Archiv Kemi*, 1963, **21**, 357.
18 R. Enjalbert and J. Galy, *Acta Cryst. C*, 1986, **42**, 1986.
19 K. A. Wilhelmi, K. Waltersson and L. Kihlborg, *Acta Chemica Scandinavica*, 1971, **25**, 2675.
20 Y. Oka, T. Yao, N. Yamamoto, Y. Ueda and A. Hayashi, *J. Solid State Chem.*, 1993, **105**, 271.
21 C. Delmas, H. Cognac-Auradou, J. M. Cocciantelli, M. Menetrier and J. P. Doumerc, *Solid State Ionics*, 1994, **69**, 257.
22 C. Leger, S. Bach, P. Soudan and J.-P. Pereira-Ramos, *J. Electrochem. Soc.*, 2005, **152**, A236.
23 J. Livage, *Chem. Mater.*, 1991, **3**, 578.
24 J. Livage, *Coord. Chem. Rev.*, 1998, **178–180**, 999.
25 Y. Wang and G. Cao, *Chem. Mater.*, 2006, **18**, 2787.
26 D. R. Rolison and B. Dunn, *J. Mater. Chem.*, 2001, **11**, 963.
27 D. B. Le, S. Passerini, A. L. Tipton, B. B. Owens and W. H. Smyrl, *J. Electrochem. Soc.*, 1995, **142**, L102.
28 D. B. Le, S. Passerini, J. Guo, J. Ressler, B. B. Owens and W. H. Smyrl, *J. Electrochem. Soc.*, 1996, **143**, 2099.
29 K. Sudoh and H. Hirashima, *J. Non-Cryst. Solids*, 1992, **147/148**, 386.
30 F. Chaput, B. Dunn, P. Fuqua and K. Salloux, *J. Non-Cryst. Solids*, 1995, **188**, 11.
31 W. Dong, D. Rolison and B. Dunn, *Electrochem. Solid-State Lett.*, 2000, **3**, 457.
32 P. Aldebert, N. Baffier, N. Gharbi and J. Livage, *Mater. Res. Bull.*, 1981, **16**, 669.
33 B. B. Owens, S. Passerini and W. H. Smyrl, *Electrochim. Acta*, 1999, **45**, 215.
34 W. H. Smyrl, S. Passerini, M. Giorgetti, F. Coustier, M. M. Fay and B. B. Owens, *J. Power Sources*, 2001, **97–98**, 469.
35 M. Giorgetti, S. Passerini, W. H. Smyrl and M. Berrettoni, *Inorg. Chem.*, 2000, **39**, 1514.
36 V. Petkov, P. N. Trikalitis, E. S. Bozin, S. J. L. Billinge, T. Vogt and M. G. Kanatzidis, *J. Am. Chem. Soc.*, 2002, **124**, 10157.
37 H.-K. Park, W. H. Smyrl and M. D. Ward, *J. Electrochem. Soc.*, 1995, **142**, 1068.
38 W. Dong, J. S. Sakamoto and B. Dunn, *Sci. Technol. Adv. Mat.*, 2003, **4**, 3.
39 S. Passerini, D. B. Le, W. H. Smyrl, M. Berrettoni, R. Tossici, R. Marassi and M. Giorgetti, *Solid State Ionics*, 1997, **104**, 195.
40 M. S. Whittingham, Y. Song, S. Lutta, P. Y. Zavalij and N. A. Chernova, *J. Mater. Chem.*, 2005, **15**, 3362.
41 S. Passerini, W. H. Smyrl, M. Berrettoni, R. Tossici, M. Rosolen, R. Marassi and F. Decker, *Solid State Ionics*, 1996, **90**, 5.
42 M. Giorgetti, S. Passerini and W. H. Smyrl, *Proc. Electrochem. Soc.*, 2000, **99–24**, 192.
43 M. Giorgetti, S. Passerini and W. H. Smyrl, *Chem. Mater.*, 1999, **11**, 2257.
44 E. Frabetti, E. G. A. Deluga, W. H. Smyrl, M. Giorgetti and M. Berrettoni, *J. Phys. Chem. B*, 2004, **108**, 3765.
45 L. Tipton, S. Passerini, B. B. Owens and W. H. Smyrl, *J. Electrochem. Soc.*, 1996, **143**, 3473.
46 G. Sudant, E. Baudrin, B. Dunn and J.-M. Tarascon, *J. Electrochem. Soc.*, 2004, **151**, A666.
47 N. Mansour, P. H. Smith, W. M. Baker, M. Balasubramanian and J. McBreen, *Electrochim. Acta*, 2002, **47**, 3151.
48 K. West, B. Zachau-Christiansen, T. Jacobsen and S. Skaarup, *Electrochim. Acta*, 1993, **38**, 1215.
49 F. Coustier, J.-M. Lee, S. Passerini and W. H. Smyrl, *Solid State Ionics*, 1999, **116**, 279–291.
50 N. Mansour, S. Dallek, P. H. Smith and W. M. Baker, *J. Electrochem. Soc.*, 2002, **149**, A1589.
51 N. Mansour, P. H. Smith, W. M. Baker, M. Balasubramanian and J. McBreen, *J. Electrochem. Soc.*, 2003, **150**, A403.
52 N. Mansour, P. H. Smith, M. Balasubramanian and J. McBreen, *J. Electrochem. Soc.*, 2005, **152**, A1312.
53 J. S. Sakamoto and B. Dunn, *J. Electrochem. Soc.*, 2002, **149**, A26–A30.
54 J. S. Sakamoto and B. Dunn, *J. Mater. Chem.*, 2002, **12**, 2859.
55 Y. S. Cohen and D. Aurbach, *Electrochem. Comm.*, 2004, **6**, 536.
56 D. B. Le, S. Passerini, F. Coustier, J. Guo, T. Soderstrom, B. B. Owens and W. H. Smyrl, *Chem. Mater.*, 1998, **10**, 682.
57 P. E. Tang, J. S. Sakamoto, E. Baudrin and B. Dunn, *J. Non-Cryst. Solids*, 2004, **350**, 67.
58 M. Bervas, L. C. Klein and G. G. Amatucci, *Solid State Ionics*, 2005, **176**, 2735.
59 H.-K. Park, *Solid State Ionics*, 2005, **176**, 307.
60 Y. Lu, M. Wei, Z. Wang, D. G. Evans and X. Duan, *Electrochem. Commun.*, 2004, **6**, 672.
61 E. Potiron, A. Le Gal La Salle, A. Verbaere, Y. Piffard, D. Guyomard and M. Tournoux, *J. Phys. Chem. Solids*, 2001, **62**, 1447.
62 G. G. Amatucci, F. Badway, A. Singhal, B. Beaudoin, G. Skandan, T. Bowmer, I. Plitz, N. Pereira, T. Chapman and R. Jaworski, *J. Electrochem. Soc.*, 2001, **148**, A940.
63 M. Giorgetti, S. Mukerjee, S. Passerini, J. McBreen and W. H. Smyrl, *J. Electrochem. Soc.*, 2001, **148**, A768.
64 M. Giorgetti, M. Berrettoni and W. H. Smyrl, *Chem. Mater.*, 2007, **19**, 5991.

65 P. E. Stallworth, F. S. Johnson, S. G. Greenbaum, S. Passerini, J. Flowers and W. Smyrl, *J. Appl. Phys.*, 2002, **92**, 3839.
66 G. P. Holland, D. A. Buttry and J. L. Yarger, *Chem. Mater.*, 2002, **14**, 3875.
67 G. P. Holland, J. L. Yarger, D. A. Buttry, F. Huguenin and R. M. Torresi, *J. Electrochem. Soc.*, 2003, **150**, A1718.
68 J. Galy, *J. Solid State Chem.*, 1992, **100**, 229.
69 Y. Oka, T. Yao and N. Yamamoto, *J. Solid State Chem.*, 1997, **132**, 323.
70 P. Y. Zavalij, F. Zhang and M. S. Whittingham, *Solid State Sci.*, 2002, **4**, 591.
71 P. Y. Zavalij and M. S. Whittingham, *Abstracts of the XVII International Union of Crystallography Congress*, Seattle, WA, USA, 1996.
72 P. Y. Zavalij and M. S. Whittingham, *The Rigaku Journal*, 2004, **21**, 2.
73 F. Zhang, P. Y. Zavalij and M. S. Whittingham, *Mater. Res. Bull.*, 1997, **32**, 701.
74 F. Zhang, P. Y. Zavalij and M. S. Whittingham, *Mater. Res. Soc. Symp. Proc.*, 1998, **496**, 367.
75 F. Zhang and M. S. Whittingham, *Electrochem. Commun.*, 2000, **2**, 69.
76 C. Torardi, C. R. Miao, M. E. Lewittes and Z. Li, *Proc. Electrochem. Soc.*, 2000, **2000–21**, 68.
77 C. Torardi, C. R. Miao, M. E. Lewittes and Z. Li, *J. Solid State Chem.*, 2002, **163**, 93.
78 M. G. Kanatzidis, C.-G. Wu, H. O. Marcy and C. R. Kannewurf, *J. Am. Chem. Soc.*, 1989, **111**, 4139.
79 F. Leroux, B. E. Koene and L. F. Nazar, *J. Electrochem. Soc.*, 1996, **143**, L181.
80 H. P. Wong, B. C. Dave, F. Leroux, J. Harreld, B. Dunn and L. F. Nazar, *J. Mater. Chem.*, 1998, **8**, 1019.
81 G. R. Goward, F. Leroux and L. F. Nazar, *Electrochim. Acta*, 1998, **43**, 1307.
82 J. H. Harreld, B. Dunn and L. F. Nazar, *Int. J. Inorg. Mater.*, 1999, **1**, 135.
83 S. T. Lutta, H. Dong, P. Y. Zavalij and M. S. Whittingham, *Mater. Res. Bull.*, 2005, **40**, 383.
84 S. T. Lutta, H. Dong, P. Y. Zavalij and M. S. Whittingham, *Mater. Res. Soc. Symp. Proc.*, 2004, **788**, L5.5.1.
85 S. T. Lutta, PhD Thesis, Binghamton University (2004).
86 C. Ban and M. S. Whittingham, *Solid State Ionics*, 2008, **179**, 1721.
87 C. Ban, PhD Thesis, Binghamton University (2008).
88 C. Ban, N. A. Chernova and M. S. Whittingham, *Electrochem. Commun.*, 2009, **11**, 522.
89 P. Viswanathamurthi, N. Bhattarai, H. Y. Kim and D. R. Lee, *Script. Mater.*, 2003, **49**, 577.
90 P. M. Ajayan, O. Stephan, P. Redlich and C. Colliex, *Nature*, 1995, **375**, 564.
91 J. Patrissi and C. R. Martin, *J. Electrochem. Soc.*, 1999, **146**, 3176.
92 C. R. Sides, N. Li, C. J. Patrissi, B. Scrosati and C. R. Martin, *Mater. Res. Soc. Bull.*, 2002, **27**, 604.
93 C. J. Patrissi and C. R. Martin, *J. Electrochem. Soc.*, 2001, **148**, A1247.
94 K. Takahashi, S. J. Limmer, Y. Wang and G. Cao, *J. Phys. Chem. B*, 2004, **108**, 9795.
95 K. West, B. Zachau-Christiansen and T. Jacobsen., *Electrochim. Acta*, 1983, **28**, 1829.
96 W. Murphy, P. A. Christian, F. J. DiSalvo and J. N. Carides, *J. Electrochem. Soc.*, 1979, **126**, 497.
97 S. Kachi, T. Takada and K. Kosuge, *J. Phys. Soc. Japan*, 1963, **18**, 1839.
98 P. D. Dernier, *Mater. Res. Bull.*, 1974, **9**, 955.
99 C. Gossard, F. J. DiSalvo, L. C. Erich, J. P. Remeika, H. Yasuoka, K. Kosuge and S. Kachi, *Phys. Rev. B*, 1974, **10**, 4178.
100 K. Kawashima, Y. Ueda, K. Kosuge and S. Kachi, *J. Cryst. Growth*, 1974, **26**, 321.
101 J. Höwing, T. Gustafsson and J. O. Thomas, *Acta Cryst. B*, 2003, **59**, 747.
102 W. Murphy, P. A. Christian, F. J. DiSalvo, J. N. Carides and J. V. Waszczak, *J. Electrochem. Soc.*, 1981, **128**, 2053.
103 K. West, B. Zachau-Christiansen, T. Jacobsen and S. J. Atlung, *J. Power Sources*, 1985, **14**, 235.
104 T. Gustafsson, J. O. Thomas, R. Koksbang and G. C. Farrington, *Electrochim. Acta*, 1992, **37**, 1639.
105 P. E. Stallworth, S. Kostov, M. L. denBoer, S. G. Greenbaum and C. Lampe-Önnerud, *J. Appl. Phys.*, 1998, **83**, 1274.
106 H. Björk, S. Lidin, T. Gustafsson and J. O. Thomas, *Acta Cryst.*, 2001, **B57**, 759.
107 O. Bergström, T. Gustafsson and J. O. Thomas, *Acta Cryst.*, 1997, **C53**, 528.
108 O. Bergström, T. Gustafsson and J. O. Thomas, *Acta Cryst.*, 1998, **C54**, 1204.
109 O. Bergström, T. Gustafsson and J. O. Thomas, *Solid State Ionics*, 1998, **110**, 179.
110 J. Barker, E. S. Saidi and M. Y. Saidi, *Electrochim. Acta*, 1995, **40**, 949.
111 D. Kuller and B. Kapfer, in *Proceedings of the 38th Power Sources Conference*, Cherry Hill, NJ, June 1998, p. 282.
112 R. J. Brodd, K. R. Bullock, R. A. Leising, R. L. Middaugh, J. R. Miller and E. Takeuchi, *J. Electrochem. Soc.*, 2004, **151**, K1.
113 C. Leger, S. Bach and J.-P. Pereira-Ramos, *J. Solid State Electrochem.*, 2007, **11**, 71.
114 T. Chirayil, P. Zavalij and M. S. Whittingham, *Solid State Ionics*, 1996, **84**, 163.
115 J. DiSalvo, D. W. Murphy and J. V. Waszczak, *Synth. Met.*, 1979, **1**, 29.
116 D. W. Murphy, F. J. DiSalvo, J. N. Carides and J. V. Waszczak, *Mater. Res. Bull.*, 1978, **13**, 1395.
117 B. C. H. Steele, *J. Phys., Colloq.*, 1978, **C2**, 198.
118 D. Muñoz-Rojas and E. Baudrin, *Solid State Ionics*, 2007, **178**, 1268.
119 F. Theobald, R. Cabala and J. Bernard, *J. Solid State Chem.*, 1976, **17**, 431.
120 C. Tsang and A. Manthiram, *J. Electrochem. Soc.*, 1997, **144**, 520.
121 B. Zachau-Chistiansen, K. West, T. Jacobsen and S. Skaarup, *Solid State Ionics*, 1992, **53–56**, 364.
122 W. Li, J. R. Dahn and D. S. Wainwright, *Science*, 1994, **264**, 1115.
123 W. Li and J. R. Dahn, *J. Electrochem. Soc.*, 1995, **142**, 1742.
124 M. Zhang and J. R. Dahn, *J. Electrochem. Soc.*, 1996, **143**, 2730.
125 M. Kannan and A. Manthiram, *Solid State Ionics*, 2003, **159**, 265.
126 W. Chen, J. Peng, L. Mai, H. Yu and Y. Qi, *Chem. Lett.*, 2004, **33**, 1366.
127 F. Zhou, X. Zhao, H. Xu and C. Yuan, *Chem. Lett.*, 2006, **35**, 1280.
128 E. Baudrin, G. Sudant, D. Larcher, B. Dunn and J.-M. Tarascon, *Chem. Mater.*, 2006, **18**, 4369.
129 M. E. Spahr, P. Stoschitzki-Bitterli, R. Nesper, M. Müller, F. Krumeich and H. U. Nissen, *Angew. Chem. Int. Ed.*, 1998, **37**, 1263.
130 H.-J. Muhr, F. Krumeich, U. P. Schönholzer, F. Bieri, M. Niederberger, L. J. Gauckler and R. Nesper, *Adv. Mater.*, 2000, **12**, 231.
131 F. Krumeich, H.-J. Muhr, M. Niederberger, F. Bieri, B. Schnyder and R. Nesper, *J. Am. Chem. Soc.*, 1999, **121**, 8324.
132 M. Niederberger, H.-J. Muhr, F. Krumeich, F. Bieri, D. Günther and R. Nesper, *Chem. Mater.*, 2000, **12**, 1995.
133 A. Dobley, K. Ngala, S. Yang, P. Y. Zavalij and M. S. Whittingham, *Chem. Mater.*, 2001, **13**, 4382.
134 M. E. Spahr, P. Stoschitzki-Bitterli, R. Nesper, O. Haas and P. Novák, *J. Electrochem. Soc.*, 1999, **146**, 2780.
135 J. M. Reinoso, H.-J. Muhr, F. Krumeich, F. Bieri and R. Nesper, *Helvetica Chimica Acta.*, 2000, **83**, 1724.
136 X. Wang, L. Liu, R. Bontchev and A. J. Jacobson, *Chem. Commun.*, 1998, 1009.
137 V. Petkov, P. Y. Zavalij, S. Lutta, M. S. Whittingham, V. Parvanov and S. Shastri, *Phys. Rev. B*, 2004, **69**, 085410.
138 M. Wörle, F. Krumeich, F. Bieri, H. Muhr and R. Nesper, *Z. Anorg. Allg. Chem.*, 2002, **628**, 2778.
139 M. Roppolo, C. B. Jacobs, S. Upreti, N. A. Chernova and M. S. Whittingham, *J. Mater. Sci.*, 2008, **43**, 4742.
140 C. O'Dwyer, D. Navas, V. Lavayen, E. Benavente, M. A. Santa Ana, G. Gonzalez, S. B. Newcomb and C. M. Sotomayor Torres, *Chem. Mater.*, 2006, **18**, 3016.
141 L. Krusin-Elbaum, D. M. Newns, H. Zeng, V. Derycke, J. Z. Sun and R. Sandstrom, *Nature*, 2004, **431**, 627.
142 E. Vavilova, I. Hellmann, V. Kataev, C. Täschner, B. Büchner and R. Klingeler, *Phys. Rev. B*, 2006, **73**, 144417.
143 C. Jacobs, M. Roppolo, K. Butterworth, C. Ban, N. A. Chernova and M. S. Whittingham, *Mater. Res. Soc. Proc.*, 2007, **988E**, QQ03.
144 J. Cao, J. L. Musfeldt, S. Mazumdar, N. A. Chernova and M. S. Whittingham, *Nano Lett.*, 2007, **7**, 2351.

145 S. Nordlinder, K. Edström and T. Gustafsson, *Electrochem. Solid-State Lett.*, 2001, **4**, A129.
146 D. G. Wickham, *J. Inorg. Nucl. Chem.*, 1965, **27**, 1939.
147 G. Pistoia, M. Pasquali, G. Wang and L. Li, *J. Electrochem. Soc.*, 1990, **137**, 2365.
148 K. West, B. Zachau-Christiansen, S. Skaarup, Y. Saidi, J. Barker, I. I. Olsen, R. Pynenburg and R. Koksbang, *J. Electrochem. Soc.*, 1996, **143**, 820.
149 S. Panero, M. Pasquali and G. Pistoia, *J. Electrochem. Soc.*, 1983, **130**, 1226.
150 J. Kawakita, Y. Katayama, T. Miura and T. Kishi, *Solid State Ionics*, 1998, **107**, 145.
151 S. Jouanneau, A. Verbaere and D. Guyomard, *J. Solid State Chem.*, 2005, **178**, 22.
152 N. Dupré, J. Gaubicher, D. Guyomard and C. P. Grey, *Chem. Mater.*, 2004, **16**, 2725.
153 R. Benedek, M. M. Thackeray and L. H. Yang, *Phys. Rev. B*, 1999, **60**, 6335.
154 A. Brylev, O. A. Shlyakhtin, A. V. Egorov and Y. D. Tretyakov, *J. Power Sources*, 2007, **164**, 868.
155 P. Rozier, M. Morcrette, P. Martin, L. Laffont and J.-M. Tarascon, *Chem. Mater.*, 2005, **17**, 984.
156 C. C. Torardi and C. R. Miao, *Chem. Mater.*, 2002, **14**, 4430.
157 F. Théobald and R. Cabala, *C.R. Séances Acad. Sci. Ser. C*, 1970, **270**, 2138.
158 Y. Oka, T. Yao and N. Yamamoto, *J. Solid State Chem.*, 1990, **89**, 372.
159 V. Legagneur, A. L. G. L. Salle, A. Verbaere, Y. Piffard and D. Guyomard, *J. Mater. Chem.*, 2000, **10**, 2805.
160 V. Legagneur, A. L. G. L. Salle, A. Verbaere, Y. Piffard and D. Guyomard, *Electrochim. Acta.*, 2002, **47**, 1153.
161 H. Qiao, X. Zhu, Z. Zheng, L. Liu and L. Zhang, *Electrochem. Comm.*, 2006, **8**, 21.
162 K. J. Takeuchi, A. C. Marschilok, S. M. Davis, R. A. Leising and E. S. Takeuchi, *Coordination Chemistry Reviews*, 2001, **219**, 283.
163 M. Bergman, S. J. Ebel, E. S. Takeuchi and P. Keister, *J. Power Sources*, 1987, **20**, 179.
164 A. Deschanvres and B. Raveau, *C. R. Acad. Sci. Paris*, 1964, **259**, 3553.
165 P. Fleury, R. Kohlmuller and M. G. Chaudron, *C. R. Acad. Sci. Paris*, 1966, **262**, 475.
166 E. Wenda, *J. Therm. Anal.*, 1985, **30**, 879.
167 C. C. Liang, M. E. Bolster and R. M. Murphy, *US Pat.* 4310609 and 4391729, 1982.
168 W. Zandbergen, A. M. Crespi, P. M. Skarstad and J. F. Vente, *J. Solid State Chem.*, 1994, **110**, 167.
169 E. S. Takeuchi and W. C. Thiebolt, *J. Electrochem. Soc.*, 1988, **135**, 2691.
170 K. West and A. M. Crespi, *J. Power Sources*, 1995, **54**, 334.
171 F. Garcia-Alvarado and J. M. Tarascon, *Solid State Ionics*, 1994, **73**, 247.
172 J. Kawakita, Y. Katayama, T. Miura and T. Kishi, *Solid State Ionics*, 1997, **99**, 71.
173 M. Morcrette, P. Rozier, L. Dupont, E. Mugnier, L. Sannier, J. Galy and J. M. Tarascon, *Nature Mater.*, 2003, **2**, 755.
174 M. Morcrette, P. Martin, P. Rozier, H. Vezin, F. Chevallier, L. Laffont, P. Poizot and J. M. Tarascon, *Chem. Mater.*, 2005, **17**, 418.
175 C. Xiong, A. E. Aliev, B. Gnade and K. J. Balkus, *ACS Nano*, 2008, **2**, 293.
176 D. Stefanis and A. A. G. Tomlinson, *J. Mater. Chem.*, 1995, **5**, 319.
177 N. Dupré, J. Gaubicher, T. L. Mercier, G. Wallez, J. Angenault and M. Quartron, *Solid State Ionics*, 2001, **140**, 209.
178 V. Zima, M. Vlček, L. Benes, M. Casciola, L. Massinelli and R. Palombari, *Chem. Mater.*, 1996, **8**, 2505.
179 B. M. Azmi, T. Ishihara, H. Nishiguchi and Y. Takita, *J. Power Sources*, 2003, **119–121**, 273.
180 J. Barker, M. Y. Saidi and J. L. Swoyer, *J. Electrochem. Soc.*, 2004, **151**, A796.
181 S. C. Lim, J. T. Vaughey, W. T. A. Harrison, L. L. Dussak, A. J. Jacobson and J. W. Johnson, *Solid State Ionics*, 1996, **84**, 219.
182 T. A. Kerr, J. Gaubischer and L. F. Nazar, *Electrochemical and Solid State Letters*, 2000, **3**, 460.
183 Y. Song, P. Y. Zavalij and M. S. Whittingham, *J. Electrochem. Soc.*, 2005, **152**, A721.
184 M. S. Whittingham, *Mater. Res. Bull.*, 1978, **13**, 959.
185 R. Dahn, U. v. Sacken and C. A. Michal, *Solid State Ionics*, 1990, **44**, 87.
186 C. S. Johnson, J.-S. Kim, A. J. Kropf, A. J. Kahaian, J. T. Vaughey and M. M. Thackeray, *Electrochem. Commun.*, 2002, **4**, 492.
187 E. M. McCarron, *J. Chem. Soc., Chem. Commun.*, 1986, 336–338.
188 J.-D. Guo, P. Zavalij and M. S. Whittingham, *J. Solid State Chem.*, 1995, **117**, 323.
189 J.-D. Guo, P. Y. Zavalij and M. S. Whittingham, *Chem. Mater.*, 1994, **6**, 357.
190 N. Guillou, G. Ferey and M. S. Whittingham, *J. Mater. Chem.*, 1998, **8**, 2277.
191 L. Campanella and G. Pistoia, *J. Electrochem. Soc.*, 1971, **118**, 1905.
192 J. Margalit, *J. Electrochem. Soc.*, 1974, **121**, 1460–1461.
193 M. S. Whittingham, *Prog. Solid State Chem.*, 1978, **12**, 41–99.
194 F. Bonino, L. Peraldo Bicelli, B. Rivolta, M. Lazzari and F. Festorazzi, *Solid State Ionics*, 1985, **17**, 21–28.
195 J. O. Besenhard, J. Heydecke, E. Wudy, H. P. Fritz and W. Foag, *Solid State Ionics*, 1983, **8**, 61–71.
196 N. Kumagai, N. Kumagai and K. Tanno, *Electrochim. Acta.*, 1987, **32**, 1521.
197 P. Fiordiponti, G. Pistoia, C. Temperoni, M. Icovi and S. Panero, *J. Electroanal. Chem.*, 1980, **108**, 181–190.
198 A. Christian, J. N. Carides, F. J. DiSalvo and J. V. Waszczak, *J. Electrochem. Soc.*, 1980, **127**, 2315–2319.
199 C. Julien, A. Khelfa, J. P. Guesdon and A. Gorenstein, *Appl. Physics A*, 1994, **59**, 173–178.
200 C. Julien, *Ionics*, 1996, **2**, 169–178.
201 C. Julien and G. A. Nazri, *Solid State Ionics*, 1994, **68**, 111–116.
202 T. Tsumura and M. Inagaki, *Solid State Ionics*, 1997, **104**, 183–189.
203 Y. Iriyama, T. Abe, M. Inaba and Z. Ogumi, *Solid State Ionics*, 2000, **135**, 95–100.
204 J. W. Bullard and R. L. Smith, *Solid State Ionics*, 2003, **160**, 335–349.
205 J. Ramirez and A. Martinez-de la Cruz, *J. Solid State Electrochem.*, 2003, **7**, 259–263.
206 G. Guzman, B. Yebka, J. Livage and C. Julien, *Solid State Ionics*, 1996, **86–88**, 407–413.
207 G. A. Nazri and C. Julien, *Ionics*, 1996, **2**, 1.
208 A. Martinez-de la Cruz and I. Juarez Ramirez, *J. Power Sources*, 2004, **133**, 268–271.
209 M. Hashim, G. H. Wrodnigg, M. H. Askar, M. Winter, J. H. Albering and J. O. Besenhard, *Ionics*, 2002, **8**, 183–191.
210 Y.-S. Kim, H.-J. Ahn, H.-S. Shim, S. H. Nam, T.-Y. Seong and W. B. Kim, *Electrochem. Solid-State Lett.*, 2007, **10**, A180–A183.
211 M. Hashim, M. H. Askar, M. Winter, J. H. Albering and J. O. Besenhard, *Ionics*, 2007, **13**, 3–8.
212 F. Leroux, G. R. Goward, W. P. Power and L. F. Nazar, *Electrochem. Solid-State Lett.*, 1998, **1**, 255–258.
213 F. Leroux and F. Nazar, *Solid State Ionics*, 2000, **133**, 37–50.
214 W. Li, F. Cheng, Z. Tao and J. Chen, *J. Phys. Chem. B*, 2006, **110**, 119–124.
215 Z. Wen, Q. Wang and J. Li, *J. Nanosci. Nanotechnol.*, 2006, **6**, 2117–2122.
216 L. Mai, B. Hu, W. Chen, Y. Qi, C. Lao, R. Yang, Y. Dai and Z. L. Wang, *Adv. Mater.*, 2007, **19**, 3712–3716.
217 *PNGV Battery Test Manual, Revision 3*, DOE/ID10597, 2001, February.
218 K. Smith and C.-Y. Wang, *J. Power Sources*, 2006, **160**, 662.
219 G. Sudant, E. Baudrin, D. Larcher and J.-M. Tarascon, *J. Mater. Chem.*, 2005, **15**, 1263–1269.
220 G. Armstrong, A. R. Armstrong, J. Canalas and P. G. Bruce, *Electrochem. Solid-State Lett.*, 2006, **9**, A139–A143.
221 P. Polzot, S. Laruelle, S. Grugeon, L. Dupont and J.-M. Tarascon, *Nature (London)*, 2000, **407**, 496–499.
222 P. L. Taberna, S. Mitra, P. Poizot, P. Simon and J.-M. Tarascon, *Nature Materials*, 2006, **5**, 568–573.
223 H. Mahan, P. A. Parilla, K. M. Jones and A. C. Dillon, *Chem. Phys. Lett.*, 2005, **413**, 88–94.
224 S.-H. Lee, Y.-H. Kim, R. Deshpande, P. A. Parilla, E. Whitney, D. T. Gillaspie, K. M. Jones, A. H. Mahan, S. B. Zhang and A. C. Dillon, *Adv. Mat.*, 2008, **20**, 3627–3632.
225 K. Deb, *Phil. Mag*, 1973, **27**, 801–822.
226 S.-H. Lee, H. M. Cheong, J.-G. Zhang, A. Mascarenhas, D. K. Benson and S. K. Deb, *Appl. Phys. Lett.*, 1999, **74**, 242–244.

227 G. Granqvist, *Handbook of Inorganic Electrochromic Materials*, Elsevier, New York, 1995.
228 M. Lampert, *Solar Energy Mat. and Solar Cells*, 2003, **76**, 489–499.
229 M. Lampert, *Glass Sci. and Tech.*, 2002, **75**, 244–252.
230 S.-H. Lee, H. M. Cheong, P. Liu, D. Smith, C. E. Tracy, A. Mascarenhas, J. R. Pitts and S. K. Deb, *J. Appl. Phys.*, 2000, **88**, 3076–3078.
231 M. Grätzel, *Nature*, 2001, **409**, 575–576.
232 S.-H. Lee, R. Deshpande, P. A. Parilla, K. M. Jones, B. To, A. H. Mahan and A. C. Dillon, *Adv. Mat.*, 2006, **18**, 763–766.
233 H. Lee, H. M. Cheong, C. E. Tracy, A. Mascarenhas, A. W. Czanderna and S. K. Deb, *Appl. Phys. Lett.*, 1999, **75**, 1541–1543.
234 C. Bechinger, M. S. Burdis and J. G. Zhang, *Solid State Comm.*, 1997, **101**, 753.
235 S. Sun and P. H. Hollway, *J. Vac. Sci. Tech. A*, 1984, **2**, 336.
236 K. Deb, *Solar Energy Mat. and Solar Cells*, 1995, **39**, 191–201.
237 Z. Hussain, *J. Electronic Mat.*, 2002, **31**, 615–630.
238 M. S. Monk, T. Ali and R. D. Partridge, *Solid State Ionics*, 1995, **80**, 75–85.
239 H. Lee, M. J. Seong, C. E. Tracy, A. Mascarenhas, J. R. Pitts and S. K. Deb, *Solid State Ionics*, 2002, **147**, 129–133.
240 B. Reichman and A. J. Bard, *J. Electrochem. Soc.*, 1979, **126**, 583.
241 N. Miyata and S. Akiyoshi, *J. Appl. Phys.*, 1985, **58**, 1651–1655.
242 J. Scarminio, A. Lourenco and A. Gorenstein, *Thin Solid Films*, 1997, **302**, 66–70.
243 A. Gorenstein, J. Scarminio and A. Lourenco, *Solid State Ionics*, 1996, **86–88**, 977–981.
244 N. Baba, S. Morisaki and N. Nishiyama, *Jap. J. Appl.Phys. Part 2-Lett.*, 1984, **23**, L638–L639.
245 K. Hinokuma, A. Kishimoto and T. Kudo, *J. Electrochem. Soc.*, 1994, **141**, 876–879.
246 Y. Zhang, S. Kuai, Z. Wang and X. Hu, *Appl. Surf. Sci.*, 2000, **165**, 56–59.
247 M. Yahaya, M. M. Salleh and I. A. Talib, *Solid State Ionics*, 1998, **115**, 421–423.
248 R. Sivakumar, M. Jayachandran and C. Sanjeeviraja, *Surface Engineering*, 2004, **20**, 385.
249 R. Sivakumar, P. Manisankar, M. Jayachandran and C. Sanjeeviraja, *Solar Energy Mat. and Solar Cells*, 2006, **90**, 2438–2448.
250 J. N. Yao, Y. A. Yang and B. H. Loo, *J. Phys. Chem. B*, 1998, **102**, 1856–1860.
251 A. Donnadieu, D. Davazoglou and A. Abdellaoui, *Thin Solid Films*, 1988, **164**, 333–338.
252 D. Belanger and G. Laperriere, *Chem. Mat.*, 1990, **2**, 484–486.
253 A. Guerfi, R. W. Paynter and L. H. Dao, *J. Electrochem. Soc.*, 1995, **142**, 3457–3464.
254 M. McEvoy, K. J. Stevenson, J. T. Hupp and X. J. Dang, *Langmuir*, 2003, **19**, 4316–4326.
255 V. Hornebecq, Y. Mastai, M. Antonietti and S. Polarz, *Chem. Mat.*, 2003, **15**, 3586–3593.
256 S. Hsu, C. C. Chan, H. T. Huang, C. H. Peng and W. C. Hsu, *Thin Solid Films*, 2008, **516**, 4839–4844.

